

Colloids as model systems for metals and alloys: a case study of crystallization

This article has been downloaded from IOPscience. Please scroll down to see the full text article.

2010 J. Phys.: Condens. Matter 22 153101

(<http://iopscience.iop.org/0953-8984/22/15/153101>)

[The Table of Contents](#) and [more related content](#) is available

Download details:

IP Address: 129.247.247.239

The article was downloaded on 10/03/2010 at 11:40

Please note that [terms and conditions apply](#).

TOPICAL REVIEW

Colloids as model systems for metals and alloys: a case study of crystallization

Dieter M Herlach, Ina Klassen, Patrick Wette and Dirk Holland-Moritz

Institut für Materialphysik im Weltraum, Deutsches Zentrum für Luft- und Raumfahrt (DLR), 51147 Köln, Germany

Received 7 December 2009

Published 9 March 2010

Online at stacks.iop.org/JPhysCM/22/153101

Abstract

Metallic systems are widely used as materials in daily human life. Their properties depend very much on the production route. In order to improve the production process and even develop novel materials a detailed knowledge of all physical processes involved in crystallization is mandatory. Atomic systems like metals are characterized by very high relaxation rates, which make direct investigations of crystallization very difficult and in some cases impossible. In contrast, phase transitions in colloidal systems are very sluggish and colloidal suspensions are optically transparent. Therefore, colloidal systems are often discussed as model systems for metals. In the present work, we study the process of crystallization of charged colloidal systems from the very beginning. Charged colloids offer the advantage that the interaction potential can be systematically tuned by a variation of the particle number density and the salt concentration. We use light scattering and ultra-small angle x-ray scattering to investigate the formation of short-range order in the liquid state even far from equilibrium, crystal nucleation and crystal growth. The results are compared with those of equivalent studies on metallic systems. They are critically assessed as regards similarities and differences.

(Some figures in this article are in colour only in the electronic version)

Contents

1. Introduction	1	5.2. Crystal nucleation in colloidal suspensions	11
2. Experimental details	2	6. Interfacial energy and Turnbull plots of colloids and metals	14
2.1. Preparation of charge stabilized colloidal suspensions	2	6.1. Metallic systems	14
2.2. Multipurpose light scattering setup	3	6.2. Results of modelling and simulations	15
2.3. Ultra-small angle x-ray scattering (USAXS)	4	6.3. Colloidal suspensions	16
2.4. Determination of the difference of chemical potential of liquid and solid state	5	7. Summary	18
3. Phase diagram of charged stabilized colloidal suspensions	6	Acknowledgments	19
4. Short-range order of colloids in the fluid state	7	References	19
4.1. Structure factor and its change with metastability	7		
4.2. Comparison with undercooled melts of metals	9	1. Introduction	
5. Crystal nucleation in liquid state of colloidal suspensions	10	Solidification of liquids is one of the most important phase transformations. The liquid phase is the parent from which most of the materials of daily human life ranging from isolators via semiconductor materials to metals and alloys are produced. The physical and chemical properties of the as solidified materials depend in a crucial way on the conditions	
5.1. Determination of the nucleation rate from measured structure factors	10		

of crystallization and solidification. In order to improve the production processes and even to develop novel materials with extraordinary properties a detailed knowledge of the physical processes involved in crystallization is mandatory. Crystallization is initiated by crystal nucleation followed by growth of primarily formed crystals. The crystal nucleation preselects the crystallographic phase stable or metastable while the growth controls the development of microstructure [1].

Nucleation plays a decisive role in many different phase transformations. Even though a great variety of models ranging from physical atomistic to pure phenomenological models have been developed to understand and even to quantitatively describe nucleation processes, experimental results do not cover the entire spectrum of phenomena involved in nucleation [2]. The direct observation of the nucleation process in atomic and molecular systems suffers from the fact that the materials of interest are often non-transparent and relaxation of atoms or molecules is very fast. Their vibration frequencies range up to 10^{13} Hz comparable with the Debye frequency. Also, the process of crystal growth in particular in bulk systems is hard to experimentally observe. The kinetics of the advancement of a solid/liquid interface is essentially governed by the atomic attachment kinetics with which atoms from the liquid state are integrated into the solid state of crystalline order. Also the atomic velocities in front of the interface can range up to the sound velocity as their upper physical limit. These limitations are overcome if model systems either for computer simulations and/or in reality are investigated. However, in this case, it is decisive to find detailed insight to what extent such model systems can be directly compared to real systems of metals and alloys. Recently, colloidal suspensions have been frequently discussed for their potential use as model systems for atomic and/or molecular systems [3].

Colloidal suspensions consist of mesoscopic particles (about 10 nm–10 μ m in size) dispersed in a carrier fluid-like water or oil. Therefore, Brownian motion governs the movement of colloidal particles. Monodisperse spherical colloidal particles suspended in viscous fluids spontaneously form so-called colloidal fluids or solids, if the experimentally variable interaction between the particles is strong enough. These highly correlated systems became widely recognized as model systems for condensed matter physics. The phase behaviour of colloidal spheres, in general, and the formation of colloidal crystals, in particular, have been studied extensively for several decades. Investigations include hard spheres, charged spheres and entropically attractive systems and are guided by valuable instrumental and theoretical developments.

A great advantage of charged colloidal suspensions as model systems is the possibility to tune the interaction potential opposite to atomic or molecular systems where the interaction potential is fixed for a selected system. In dependence on the interaction colloidal suspensions show a variety of different phases with a fluid, solid crystals of bcc or fcc/hcp structure and even glassy morphology. So far the colloidal particles can be considered as macro-atoms with inter-particle distances comparing to the wavelength of visible light and sluggish relaxation behaviour imaging atomic or molecular

systems on different time and length scales. The typical time and length scales of colloidal systems allow for time-resolved observations of solidification with easily manageable experimental techniques.

The present work evaluates charged colloidal systems as model systems for crystallization of metals and alloys. Different stages of crystallization are considered starting with short-range ordering in the metastable undercooled liquid state, crystal nucleation behaviour, crystal growth and phase behaviour. The experimental results obtained from colloidal suspensions are related to equivalent results of computer simulations and experiments on metals and alloys. The behaviour of the physically different systems of colloidal suspensions and metals are compared with each other and are critically assessed with respect to common behaviour and physical discrepancies.

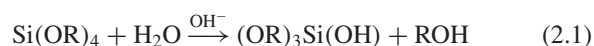
2. Experimental details

2.1. Preparation of charge stabilized colloidal suspensions

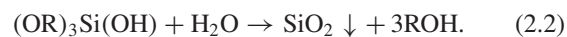
In the present work charged colloidal suspensions of silica particles dissolved in ultra-pure water have been investigated. For measurements we used two different batches with particle diameters of 77 nm (Si77) and 84 nm (Si84) small enough that Brownian motion avoids sedimentation in the gravitational field. We choose silica particles for several reasons. This particle species gives the possibility to change the interaction varying three parameters: the particle charge Z , the salt concentration c and the particle concentration n . Furthermore, the silica colloids show a high scattering contrast for x-rays even at low volume fractions.

Charge stabilized colloidal silica systems were synthesized by means of a modified Stöber synthesis [4]. This method allows for the synthesis of spherical silica particles with small size polydispersity (about 5%) in a size ranging from 5 to 2000 nm.

The synthesis of the silica colloids include a hydrolysis reaction



with $R = \text{C}_2\text{H}_5$ to produce the single-hydrolyzed TEOS monomer $(\text{OR})_3\text{Si}(\text{OH})$. Subsequently, this intermediate reaction product condenses to form silica



The synthesized SiO_2 particles carry weakly acidic silanol groups (Si–OH) on the surface, which partly dissociate in a deionized water environment leaving spheres with a negative surface charge. Surface groups of particles with strong acidic end groups are fully dissociated with their maximum possible surface charge. The dissociation of silanol groups by which silica surfaces acquire a charge in contact with water is described by $\text{SiOH} \rightarrow \text{SiO}^- + \text{H}^+$.

The degree of dissociated silanol groups strongly depends on the pH of the surrounding media. To influence the surface charge of silica particles and thus the electrostatic interaction

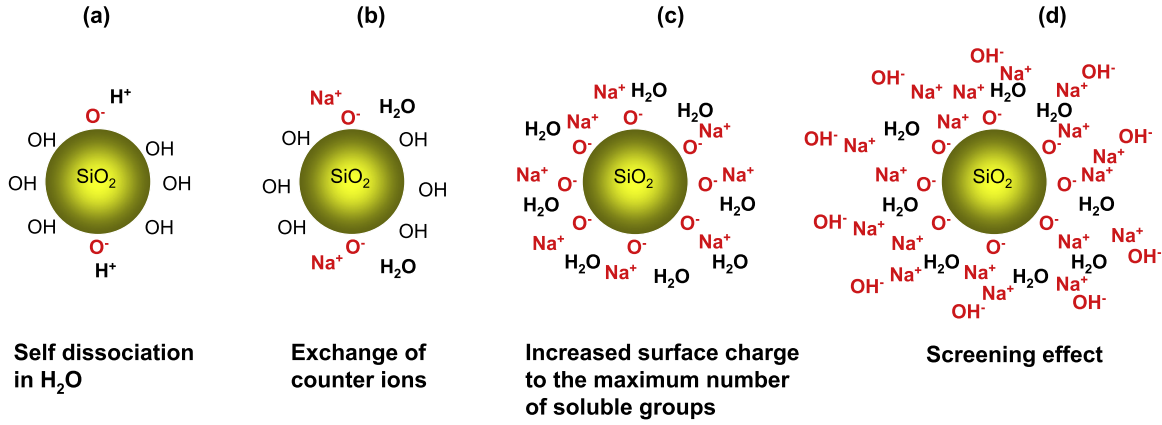


Figure 1. Control of silanol surface groups on silica particles and their interaction as a function of added NaOH with increasing NaOH concentration from left to right.

of the particles sodium hydroxide (NaOH) is added to the suspension. The addition of NaOH controls the degree of dissociation and the surface charge density [5]. By adding sodium hydroxide the counter-ion species first changes from H^+ to Na^+ followed by a charging of the silica particles due to the reaction $Si-OH + NaOH \rightarrow Si-O^- + Na^+ + H_2O$. The particles charge up until its maximum surface charge is achieved. At this point all silanol groups are used up. A further increase of the NaOH concentration, the so-called excess concentration, causes a screening of the particle surface charge and the interaction decreases. This mechanism is shown schematically in figure 1. At maximum interaction the added NaOH base is completely used up for charging up the silica particles to the maximum possible charge. Therefore, the surface charge density σ_a can be calculated from the added amount of base as [6]

$$\sigma_a = \frac{10^{-3}}{3} N_A \cdot e \cdot a \frac{c_{NaOH}}{\Phi}, \quad (2.3)$$

where N_A is Avogadro's number, e the elementary charge (in C), a the particle radius (in cm) and $\Phi = (4/3)\pi a^3$ the volume fraction of the silica particles. After complete dissociation, the excess NaOH causes a screening of the particle surface charge and the interaction decreases.

Charged colloidal systems in particular allow for a variation of the pair interaction energy through changes of particle radius a and charge Z as well of particle number density n and electrolyte concentration c . The Debye-Hückel potential in combination with an effective or renormalized charge Z^* is a widely and often successfully used concept to describe the electrostatic interaction in charged colloidal model systems and the resulting suspension properties. In highly charged colloidal monodisperse systems the pair interaction energy V can be written as

$$V(r) = \frac{(Z^*e)^2}{4\pi\epsilon_o\epsilon_r} \left(\frac{\exp(\kappa a)}{1 + \kappa a} \right)^2 \frac{\exp(-\kappa r)}{r}, \quad (2.4)$$

with the screening parameter κ

$$\kappa^2 = \frac{e^2}{\epsilon_o\epsilon_r k_B T} (n_p Z^* + 2000 N_A c)$$

$\epsilon_o\epsilon_r$ is the dielectric permittivity of the suspension and $k_B T$ is the thermal energy. The development of equation (2.4) is based upon the assumption that the electrostatic energy is much smaller than the thermal energy, $eV \ll k_B T$. The precise control of the interaction in charge stabilized systems is important for a systematic analysis of the physical properties of colloidal systems. Therefore, utilization of a continuous conditioning technique is a prerequisite for each measurement. It is used to guarantee a reproducible adjustment of interaction parameters by varying and controlling the particle number density and the counter-ion concentration [7]. The suspension is pumped peristaltically through a closed tubing system connecting an ion exchange chamber to deionize the sample, a reservoir under an inert gas atmosphere to add further suspension or water, a conductivity cell in order to determine the salt concentration and measuring cells for scattering or microscopy experiments.

As introduced above the colloid specific length scales allow for a convenient but powerful approach via optical methods like microscopy or light scattering. Both yield complementary information from real and reciprocal space. Using optical methods the structural properties, particle dynamics and the phase transition kinetics of colloidal model systems as well as the elastic properties of colloidal solids (and so the particle interaction) can be investigated with high precision allowing a full characterization of the colloidal model system.

2.2. Multipurpose light scattering setup

A specific mechanical property of colloidal solids is their softness. Due to the low particle number density n of some 10^{18} – 10^{19} m^{-3} (atomic systems $n \approx 10^{29} \text{ m}^{-3}$) the elastic moduli G are in the range of only a few Pa (atomic systems $G \approx 10^{10}$ – 10^{11} Pa). The fragility of such samples is a major constraint of investigations and it is mandatory to have a high precision light scattering setup, which enables simultaneous investigations of different properties without disturbing the sample. Therefore, a multipurpose light scattering device based upon the work by Schöpe [8–10] is used combining quasi-simultaneous static and dynamic light scattering (SLS)

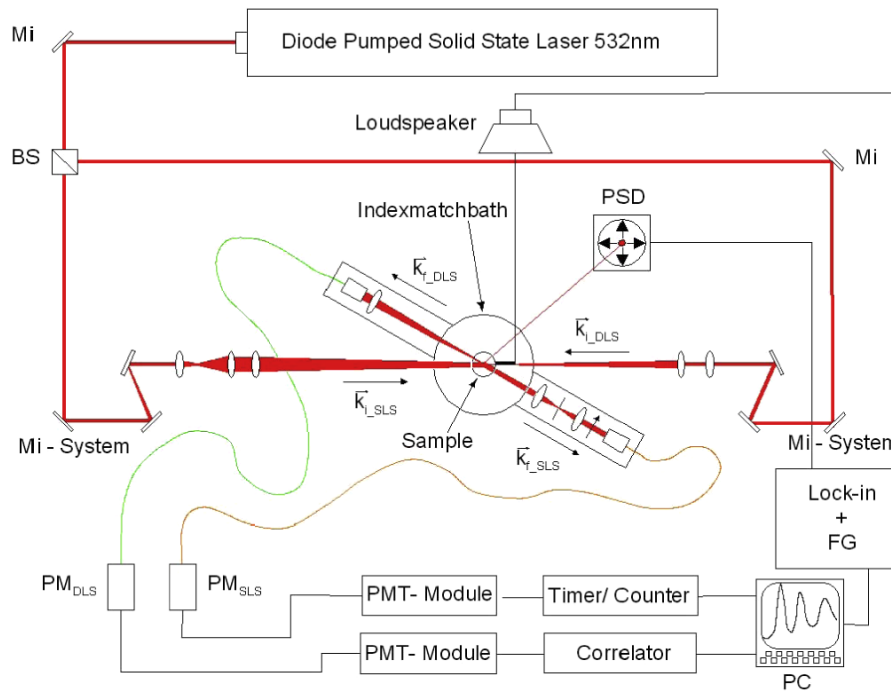


Figure 2. Multipurpose device for simultaneous measurements of static, dynamic and elastic properties of colloidal systems. The basic construction of the multipurpose device in particular the double-arm goniometer for the simultaneous measurements of static, dynamic and elastic properties was developed by Schöpe [8]. The figure includes the following abbreviations: mirror (Mi), beam splitter (BS), photomultiplier (PM) and position-sensitive detector (PSD).

and DLS) probing the structure and morphology of colloidal solids, respectively their dynamics, with torsion resonance spectroscopy (TRS) to determine the shear modulus and by this way the particle interaction.

A sketch of the apparatus is exhibited in figure 2. The setup consists of a solid state laser operating at a wavelength of 532 nm as the illumination source, two separated sending optics, a double-arm goniometer with two detection optics and an index match bath for the sample cell. The device is mounted on a vibrating-free optical table. To realize a counter-propagating illumination, the laser light is split by a beam splitter and injected into two different sending optics. The sample cell, made of quartz glass, is in the centre of the index match bath also made of quartz glass. Index matching is necessary to avoid parasitic reflections. The setup is equipped with individual illumination and detecting optics, for SLS and DLS. For SLS illumination a broad, parallel beam is required, to assure good powder averaging while for DLS the Gaussian beam waist (diameter about 100 μm) must be in the middle of the sample vial. Separated illumination and detection optics allows the use of different scattering experiments to be combined. In the sample cell both laser beams are collinear with their width and the detection optics optimized for the three different experiments. The laser beam for DLS enters from the right and is detected using the optics of the upper arm. The beam for SLS and torsion resonance detection enters from the left and is detected using the optics of the lower arm. The position-sensitive detector used to detect torsion resonances can be deliberately adjusted to collect the light of a single Bragg reflection. For torsion resonance spectroscopy (TRS) sample oscillations are excited by coupling the cell to a

loud speaker using an aluminium rod. The position-sensitive detector used for TRS is adjusted to collect scattering signals stemming from a single Bragg reflection. For further analysis of the collected light, a standard lock-in technique is used. A resonance spectrum is recorded showing response amplitude and phase lag.

Due to the fact that our silica suspensions are not optically matched, light scattering is restricted to lower particle concentration, where multiple scattering effects can be neglected. At high particle concentration, meaningful measurements by light scattering are quite difficult and x-ray scattering is an alternative method for obtaining data from the reciprocal space.

2.3. Ultra-small angle x-ray scattering (USAXS)

With increasing particle number density the colloidal suspension becomes impervious to light in the visible spectrum which makes measurements by optical light quite difficult. Change of the wavelength from the optical range to the ultraviolet range is of no help since colloidal suspensions absorb ultraviolet light. The use of x-rays opens up an extended field of scattering experiments. Since the wavelength of x-rays is much smaller than the inter-particle distance in colloidal suspensions x-ray scattering experiments have to focus on ultra-small angle x-ray scattering (USAXS). In addition, USAXS makes use of the penetration of x-rays through materials, either in the solid or liquid state. Typical scattering angles for USAXS measurements range around 1° leading to a much larger scattering vector range compared to light scattering experiments.

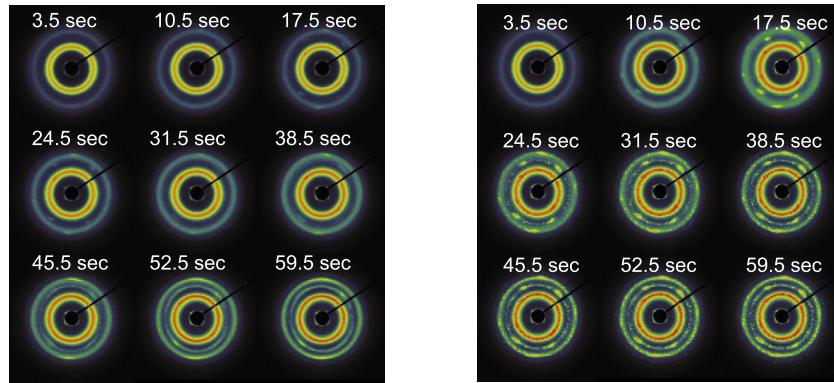


Figure 3. The sequence of nine diffraction patterns of colloidal silica suspensions with particle diameter 84 nm and particle number density $n = 113 \mu\text{m}^{-3}$ at the strongest particle interaction adjusted via the sodium hydroxide concentration $c_{\text{NaOH}} = 1.06 \times 10^{-3} \text{ mol l}^{-1}$ (left) and the weaker interaction at smaller concentration $c_{\text{NaOH}} = 0.4 \times 10^{-3} \text{ mol l}^{-1}$ (right). Homogeneous nucleation dominates in the suspension of maximum interaction. The four-fold diffraction spots on the right indicate that heterogeneous nucleation of oriented wall crystals becomes dominant if the particle interaction is weakened [12].

The beamline BW4 at HASYLAB in Hamburg is an x-ray wiggler ($N = 19$ periods, $K = 13.2$) beamline with instrumentation to perform ultra-small angle x-ray scattering especially on soft matter systems with a distance between sample and detector of 13.5 m. Details are given elsewhere [11]. The scattered beam is corrected with respect to background scattering and absorption during transmission. Figure 3 gives the scattered data of USAXS experiments with an exposure and read-out time of the detector of 3.5 s for a silica suspension (84 nm particle size, $n = 113 \mu\text{m}^{-3}$), at maximum interaction with a salty concentration $c_{\text{NaOH}} = 1.06 \times 10^{-3} \text{ mol l}^{-1}$ (left) and at weaker interaction with $c_{\text{NaOH}} = 0.4 \times 10^{-3} \text{ mol l}^{-1}$ (right). The first Debye–Scherrer rings show the broad hallow of the metastable fluid phase upon shear melting the crystal. After an exposure time of 17 s the Debye–Scherrer rings become sharper and additional rings appear, indicating the formation of a bcc polycrystalline solid from the metastable liquid. The pattern on the right of figure 3 reveals the appearance of four-fold diffraction points which are attributed to heterogeneous nucleation of an oriented wall crystal [12]. While homogeneous nucleation dominates in the suspension of maximum interaction, a weaker interaction apparently favours heterogeneous nucleation. Figure 3 demonstrates the advantage of USAXS measurements on colloidal systems that gives access of discrimination between heterogeneous and homogeneous nucleation.

Wette *et al* analysed the competitive behaviour between heterogeneous and homogeneous nucleation near a flat wall [13]. Accordingly, heterogeneous nucleation at the container walls is delayed in comparison with homogeneous nucleation within the bulk fluid. The structure factor $S(q)$ was obtained from the intensity of the diffracted beam $I(q)$ by considering the particle form factor $P(q)$ as

$$I(q) \propto I_o \cdot n \cdot P(q) \cdot S(q). \quad (2.5)$$

The particle form factor $P(q)$ was determined by proper calibration USAXS measurements [10]. I_o is the intensity of the incident beam, and n the particle number density of the suspension used.

2.4. Determination of the difference of chemical potential of liquid and solid state

At low metastability heterogeneous nucleation at the walls of the sample cell dominates and the growth velocity of colloidal crystal can be determined using time-resolved microscopy. After cessation of shear flow, a planar front of twinned bcc crystals propagates linearly with their densest packed planes parallel to the cell wall [14]. Crystallization is monitored by Bragg microscopy [15–17] in a flat flow-through cell made of quartz glass with a wall-to-wall distance of 1 mm. The cell is mounted on the stage of an inverted microscope equipped with a low-resolution objective. Images are recorded by a charged-coupled device (CCD) camera and stored in a PC for image analysis. Figure 4 (left) shows microscopic images of the crystallization of a colloidal silica suspension at low particle number density $n = 19.0 \mu\text{m}^{-3}$ with a 84 nm particle diameter taken by polarization microscopy in side view of the sample cell at different time intervals. The coloured regions represent the crystals growing in planar morphology from both sides of the cell towards the interior. The image size is of $1.00 \times 1.16 \text{ mm}^2$. The corresponding growth velocity is determined to be $9.7 \mu\text{m s}^{-1}$. The growth velocity was measured as a function of particle concentration and of the amount of added NaOH. In all cases a linear increase of the crystal dimension with time was observed indicating reaction controlled growth.

At high particle interaction between the particles, homogeneous nucleation dominates and an isotropic polycrystal arises. A typical image of a polycrystalline sample crystallized from a shear melted silica suspension at $n = 32.0 \mu\text{m}^{-3}$ is shown in figure 4 (right). The crystals appear as faceted and irregularly shaped polyheders of different colours. The facets result from crystal intersections occurring during growth. The colour differences originate from different crystal orientations.

Figure 5 shows the growth velocity at maximum particle charge as a function of the particle number density n . Firstly, the growth velocity steeply rises with n before it approaches a saturation level at large particle number density. Such behaviour is well described by the Wilson–Frenkel law

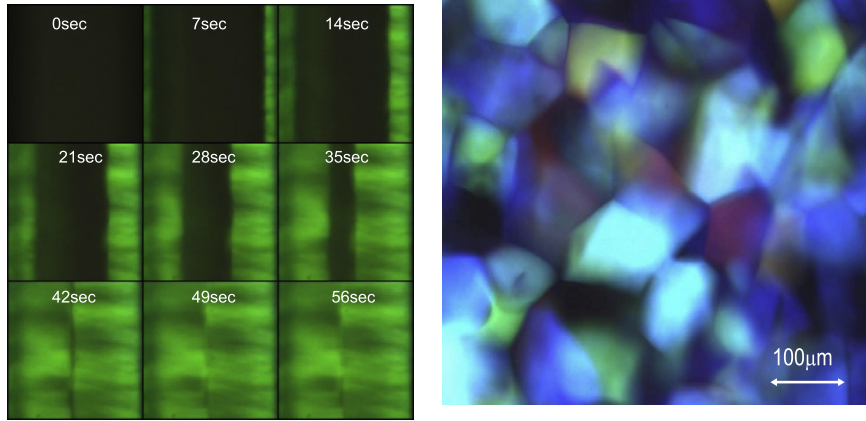


Figure 4. (Left) Growth of heterogeneously nucleated wall crystals of a colloidal silica suspension with particles of 84 nm at particle number density $n = 19.0 \mu\text{m}^{-3}$ at various time intervals starting from the top to the bottom, (right), polycrystalline solid of a silica system homogeneously nucleated within the bulk of a shear melted suspension at a particle number density $n = 26.0 \mu\text{m}^{-3}$. The different grey scales/colours are caused by light scattering from different orientation of the crystallites.

following the formalism of Aastuen *et al* [18]. Based upon investigations of Palberg [19], Stipp [20] and Broughton [21] the resulting growth velocity is described by the equation

$$v = f_0 d_i \cdot \frac{D}{d_{\text{NN}}^2} \left[1 - \exp\left(-\frac{\Delta\mu}{k_B T}\right) \right], \quad (2.6)$$

with d_i the thickness of the liquid layer, f_0 the success rate of particle attachment from the liquid impinge at the solid, D the long time self-diffusion coefficient, d_{NN} the next-nearest neighbour distance as the characteristic length scale for particle diffusion, $\Delta\mu = \mu_L - \mu_S$ the difference of chemical potential in liquid, μ_L , and in solid, μ_S , state. k_B is Boltzmann's constant and T the temperature. While the impingement factor f_0 may be smaller than 1 (not each particle jump from the liquid to the solid is successful), it is $f_0 = 1$ for pure metals with more or less metallic isotropic bonding [22], but much less $f_0 \approx 0.01$ for pure semiconductors with strong directional covalent bonding [23]. The prefactor of equation (2.6) has the dimension of a velocity and corresponds to the velocity v_∞ of the advancing solid–liquid interface at infinite driving force $\Delta\mu = \infty$. To adapt this formalism to colloidal systems, an assumption for the chemical potential difference is necessary. According to Würth *et al* [14] $\Delta\mu$ can be expressed in terms of a rescaled energy density $\Delta\mu = k_B T \cdot B \cdot \Pi^*$ with $\Pi^* = (\Pi - \Pi_F)/\Pi_F$ giving the possibility to determine $\Delta\mu$. The energy density is given as $\Pi = \alpha n V(d_{\text{NN}})$, with α being the particle coordination number, $V(d_{\text{NN}})$ is the interaction energy at nearest neighbour distance, and F denotes freezing. This approach considers both the direct linear density dependence of $\Delta\mu$ and the pair interaction energy $V(r)$. B is a fitting parameter that needs to be determined from experiment. The best fit to the data of figure 5 yields $v_\infty = (9.3 \pm 0.2) \mu\text{m s}^{-1}$ and $B = (4.69 \pm 0.67)k_B T$. Equation (2.6) describes well the experimental data with the fitting parameters as given above. The difference of the chemical potential between the liquid and solid state as a function of the particle number density shows a nearly linear dependence of $\Delta\mu$ on n , which can be extrapolated at higher particle number densities, where

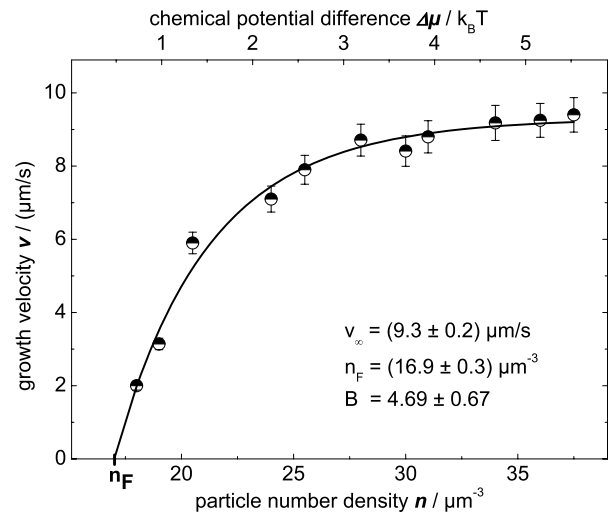


Figure 5. The growth velocity v for the Si84 system as a function of the particle number density n at maximum interaction. The solid curve is a fit of a Wilson–Frenkel law according to equation (2.6) yielding $v_\infty = (9.3 \pm 0.2) \mu\text{m s}^{-1}$ and $B = (4.69 \pm 0.67)k_B T$. The chemical potential difference $\Delta\mu$ between solid and liquid used in the upper x axes is derived using the conversion factor B .

the growth velocity is more difficult to determine due to the preference of homogeneous nucleation. The chemical potential difference is a parameter of fundamental importance to describe the degree of metastability of the fluid phase in colloidal suspensions, in the analysis of short-range order effects in the fluid state and nucleation of crystals.

3. Phase diagram of charged stabilized colloidal suspensions

Silica colloidal suspensions were investigated with particle size 77 nm (Si77) and 84 nm (Si84), respectively. Both systems are suspended in ultra-pure water. The Si84 system is characterized up to a maximum particle number density

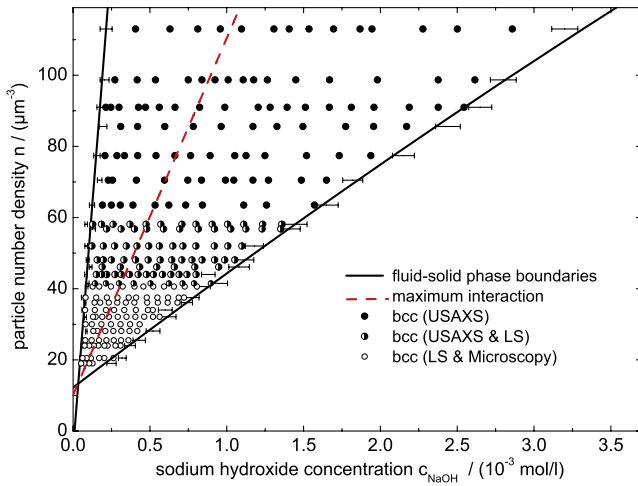


Figure 6. Phase diagram of Si84 in dependence on the particle number density and the sodium hydroxide concentration as determined by USAXS (filled circles) and light scattering (LS) (open circles). Both measurement techniques show an overlapping regime with coinciding results for n between 40 and 60 μm^{-3} . The black lines are guides to the eyes for the solid–fluid phase boundaries with an uncertainty marked by the error bars. The dashed line characterizes the region of maximum particle interaction as determined from torsion resonance spectroscopy.

$n = 113 \mu\text{m}^{-3}$ corresponding to a volume fraction $\Phi = 0.035$, while $n = 224 \mu\text{m}^{-3}$ and $\Phi = 0.053$ for Si77, respectively. Both systems show similar phase behaviour and qualitatively similar phase diagrams. The phase behaviour was investigated by USAXS (wavelength 0.138 nm) in the range of high particle number densities and by static light (wavelength 532 nm) scattering and microscopy in the range of small particle number densities. Intensity distributions as a function of the scattering vector q were used to identify the structure and, in case of crystallizing samples, determining the n -dependent lattice constant and thus, the particle number density. Figure 6 shows the phase diagram of the Si84 system, in which the particle number density n is plotted versus the concentration of sodium hydroxide c_{NaOH} . The suspension crystallizes in a bcc structure up to the largest particle number density. A crystalline phase is observed for number densities larger than $n = 18.0 \mu\text{m}^{-3}$. The crystalline region shows two fluid–solid boundaries. To the left the boundary is reached by charging the particles up at still deionized conditions. To the right it is reached by increased screening.

The horizontal error bars characterize the two-phase region of fluid and solid. The solid lines are guides to the eyes dividing the crystalline bcc from the fluid phases. The dashed line indicates the region of maximum particle charge, i.e. maximum interaction at fixed particle number density n , where all silanol groups on the particle surface are used up for the charging-up reaction. The conditions of maximum interaction are determined by measurements of the shear modulus by means of torsion resonance spectroscopy, described elsewhere in detail [9]. The conversion of the charge density at maximum interaction at each concentration results in an averaged number of silanol groups on each particle surface of $Z_{\text{bare}} = 4520 \pm 130$. The corresponding effective charge

from the shear module measurements $Z^* = 340 \pm 20$ stays constant with increasing n which was already observed for polystyrene particles under deionized conditions [24]. The determination of Z^* allows the effective interaction potential in the used colloidal model system to be calculated.

In contrast to systems of fixed particle charge [25] the Si84 system shows a re-entrant behaviour as a function of either n or c_{NaOH} . At increasing particle number density under completely deionized conditions the charge is too small to cause crystalline order. At constant c_{NaOH} an increase of n reduces the amount of NaOH available per silanol group and this first causes a decrease of screening but then a decrease of the charge density. Thus, re-entrant behaviour is given in two variables not reported previously for other systems. It is interesting to note that there is some similarity with phase behaviour of binary metallic alloys showing a retrograde in their phase diagrams as e.g. Co–Cu [26]. At fixed concentration the liquid crystallizes with decreasing temperature and re-melts partly upon further lowering the temperature until the two-phase regime completely solidifies.

4. Short-range order of colloids in the fluid state

4.1. Structure factor and its change with metastability

In the present work the short-range order of colloidal suspensions in the liquid state is investigated if the liquid is far away from equilibrium. Deviations from equilibrium are measured by $\Delta\mu$. Shear melting a crystal leaves the system in a metastable liquid state. Figure 7 shows the time evolution of the structure factor of the colloidal system from the non-equilibrium liquid state (lower curve) to the stable solid phase (upper curve) at a particle number density $n = 113 \mu\text{m}^{-3}$. The time interval between each curve corresponds to 7 s due to the integration interval of 3.5 s and the detector read-out time of 3.5 s. This assures that especially the first structure factor taken after 3.5 s corresponds to a metastable liquid state. For longer times a structural transition into a stable bcc solid phase is observed. This behaviour is representative for measurements on the metastable liquid state of colloidal suspensions.

In addition, the structure factor is investigated as a function of the particle number density and the salty concentration. By increasing the particle number density from $n = 46.1$ to $113 \mu\text{m}^{-3}$ the diffraction peaks shift to higher q -values as expected due to decreasing next-nearest neighbour distances. In all measurements on the metastable liquid state an asymmetry in the second oscillation of $S(q)$ is obvious. The asymmetry of the shoulder in the second oscillation of $S(q)$ becomes more pronounced with increasing deviation from equilibrium.

The structure factor measured by elastic scattering of x-rays reveals information in reciprocal space. In order to obtain real-space information models are required to simulate $S(q)$ and to compare the simulated $S(q)$ with the experimentally determined $S(q)$. In the present work we use the formalism of Simonet *et al* [27, 28] to analyse the structure factor $S(q)$ as measured on the colloidal suspension. This model assumes one dominant type of isolated less tightly bound structural

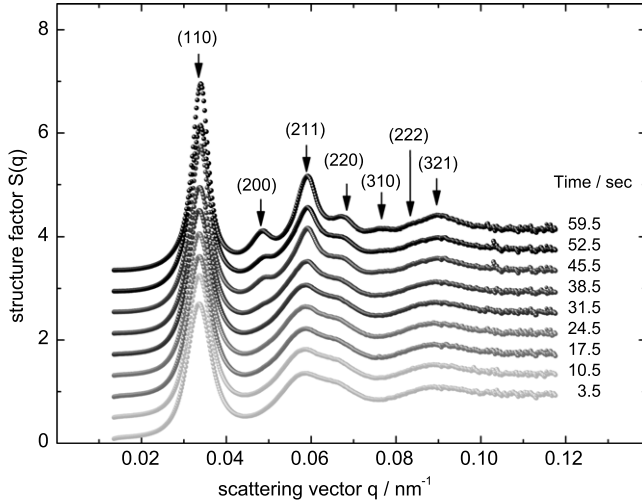


Figure 7. The time dependent static structure factors $S(q)$ for the Si84 colloidal suspension at $n = 113 \mu\text{m}^{-3}$ and maximum interaction; the colloidal crystal was shear melted leaving it in a metastable liquid state. The structure factor is measured every 7 s starting after shear melting (curve at the bottom) and during moving to equilibrium until eventually the melt crystallizes into a stable bcc solid (upper curve).

units in the liquid. Long-range inter-cluster contributions to the scattered intensity are neglected and only intra-cluster contributions are considered. This simplification is justified in the regime of large q values where the contributions of less tightly bound longer inter-cluster distances are damped out by thermal motions described by the Debye–Waller factor. Accordingly, the structure factor at large q is given by

$$S(q) = 1 + \frac{c}{Nb^2} \sum_{i,j (i \neq j)}^N b_i b_j \frac{\sin(q \langle r_{ij} \rangle)}{q \langle r_{ij} \rangle} \exp\left(-\frac{2q^2 \langle \delta r_{ij}^2 \rangle}{3}\right) \quad (4.1)$$

here, N corresponds to the number of particles in a structural unit, b_i denotes the scattering amplitude of particle i and b^2 is the average of the squares of the scattering amplitudes of all particles in one structural unit. $\langle r_{ij} \rangle$ is the mean distance between the particles i and j and $\langle \delta r_{ij}^2 \rangle$ the mean thermal variation that determines the Debye–Waller factor $\exp(-2q^2 \langle \delta r_{ij}^2 \rangle / 3)$. This model was previously successfully applied to interpret the structure factor of undercooled metallic melts measured by elastic neutron scattering [29, 30] or by elastic x-ray scattering making use of high intensity synchrotron radiation [31].

The simulation method depends on three free parameters. These are the shortest mean distance $\langle r_o \rangle$ of the particles, its mean thermal variation $\langle \delta r_o^2 \rangle$ and the fraction of particles c organized in each structural unit. For a given structure, all particle distances $\langle r_{ij} \rangle$ can be calculated from $\langle r_o \rangle$ and the mean thermal variations $\langle \delta r_{ij}^2 \rangle$ from $\langle \delta r_o^2 \rangle$ at the shortest particle distance assuming $\langle \delta r_{ij}^2 \rangle = \langle \delta r_o^2 \rangle \langle r_{ij} \rangle^2 / \langle r_o \rangle^2$. The three free parameters are adjusted such that good agreement with the experimental $S(q)$ is obtained especially at large q values. The following structures of the structural units are assumed to describe the measured $S(q)$: body centred cubic (bcc), face centred cubic (fcc) or equivalently hexagonal close

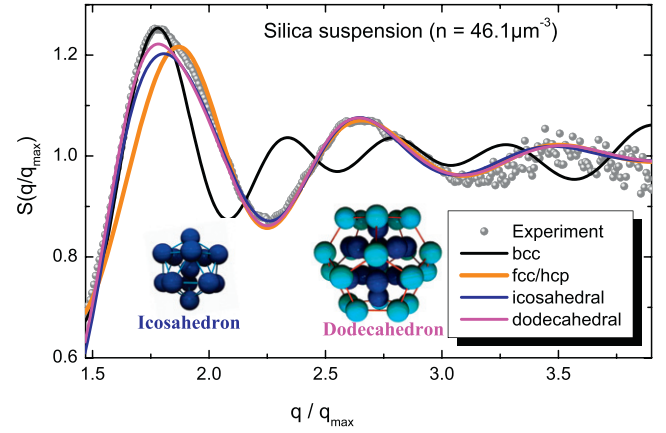


Figure 8. Simulated (lines) and measured (dots) structure factors $S(q)$ of the Si84 silica suspension in the metastable state near the maximum interaction and a particle concentration $n = 46.1 \mu\text{m}^{-3}$. Shown are data for the second and higher order oscillations. The formalism developed by Simonet *et al* [27, 28] is used to analyse the measured structure factor (circles) in the regime of large q -vectors. The silica suspension forms a stable bcc phase in the solid state under equilibrium conditions. If a short-range order of the bcc structure (black curve) is assumed, neither the position nor the shape of the asymmetric oscillation of $S(q)$ is described. The fit for a short-range order consisting of fcc clusters (orange curve) describes the measured $S(q)$ better at higher oscillations, but not the shape at lower q -values. In contrast, for an icosahedral short-range order (blue curve) a good fit of the experimental data is achieved that becomes even better, if larger dodecahedral aggregates are assumed. Dodecahedra consist of 33 elementary particles, 20 of them are located in the centre of the outer tetrahedral planes of the inner icosahedron, which consists of 13 elementary particles (cf. insets).

packed (hcp) clusters as well as icosahedral and dodecahedral short-range order of the clusters were considered. These clusters possess five-fold symmetry that is not compatible with the translational symmetry of a crystal.

Figure 8 shows simulated structure factors for a colloidal silica suspension Si84 in the metastable liquid state at maximum interaction and at particle concentration $n = 46.1 \mu\text{m}^{-3}$. For this system the deviation from equilibrium is characterized by $\Delta\mu = 6k_B T$. The silica suspension forms a stable bcc phase in the solid state.

If a short-range order of bcc structure is assumed, neither the position nor the shape of the asymmetric oscillation of the measured $S(q)$ is described. The fit for a short-range order considering fcc clusters describes the experimental data better in the range of higher q values, but not the shape of the asymmetric oscillation. In contrast, assuming an icosahedral short-range order leads to a much better agreement between simulated $S(q)$ and measured $S(q)$. It becomes even better, if larger dodecahedral aggregates are assumed to prevail in the structural units in the metastable liquid. A dodecahedron consists of 33 elementary particles, 20 of them are placed in the middle of the tetrahedral planes of an icosahedron that consists of 13 elementary particles forming 20 tetrahedral units. The same results are obtained for a Si84 colloidal suspension with $n = 113 \mu\text{m}^{-3}$ [10]. The analysis of the measured structure factors of silica colloidal suspension in the metastable state leads to the conclusion that a short-range order is dominated

by structural units of dodecahedral structure with five-fold symmetry.

The origin of the asymmetric second oscillation is understood when considering the individual contributions of each inter-atomic distance within an aggregate of fcc or hcp in comparison to an icosahedral type of local structure. In fcc or hcp structural units, the distance of the central particle to the particles on the shell and the nearest neighbour distance within the shell are the same but differ by about 5% in the case of icosahedral aggregates. The slight difference of the particle distances is responsible for the asymmetry in the second oscillation of $S(q)$. The shoulder can therefore be considered as an indication for an icosahedral short-range order. The model of Simonet *et al* certainly neglects the wealth of imperfect aggregates of five-fold symmetry [32], which are also likely to be present. But it is sufficient to yield information on the dominant type of short-range order in liquid systems.

4.2. Comparison with undercooled melts of metals

For pure metallic melts with compact local order and isotropic bonding Frank [33] hypothesized an icosahedral short-range order independent of the structure of the phases, which solidify from the melt. Frank's hypothesis was frequently used to explain the large undercoolings of pure metals as found by Turnbull [34]. It was argued that the five-fold symmetry of icosahedral short-range order must be broken before a crystal with its translational symmetry can be formed. Five-fold symmetry belongs to the crystallographically 'forbidden' point groups due to its incompatibility with translational invariance. In fact, more recently a short-range order of five-fold symmetry in undercooled metallic melts was experimentally proved by neutron [29] and x-ray [31] scattering on levitation undercooled pure metallic melts.

For both systems the formalism developed by Simonet *et al* [27, 28] was used to analyse the diffraction pattern both for the silica colloid and the pure metal of Ni. The results of simulations of the structure factor are compared with the experimental data in figure 9. The colloidal system crystallizes in a bcc structure while Ni solidifies in fcc structure. Apparently, the different structures of solid state of both systems do not have any influence on the short-range order in the liquid state. Supposing a bcc-like short-range order in the liquid state fails in describing the experimental data. A fcc type short-range order performs better but the shape and peak positions in the second oscillation do not agree with the experimental results where the significant asymmetry of a shoulder is observed. A good agreement of simulation and experiment is achieved if icosahedral aggregates of five-fold symmetry are assumed. It even becomes better assuming larger dodecahedral aggregates of five-fold symmetry. The better agreement of the simulation for icosahedral structural units in comparison with fcc aggregates is explained by considering the individual contributions of each inter-atomic distance within these clusters. The distance of the central elementary particle to the particles of the surrounding shell and the nearest neighbour distance within the shell are the same for fcc and hcp clusters and differ by about 5% compared to icosahedral

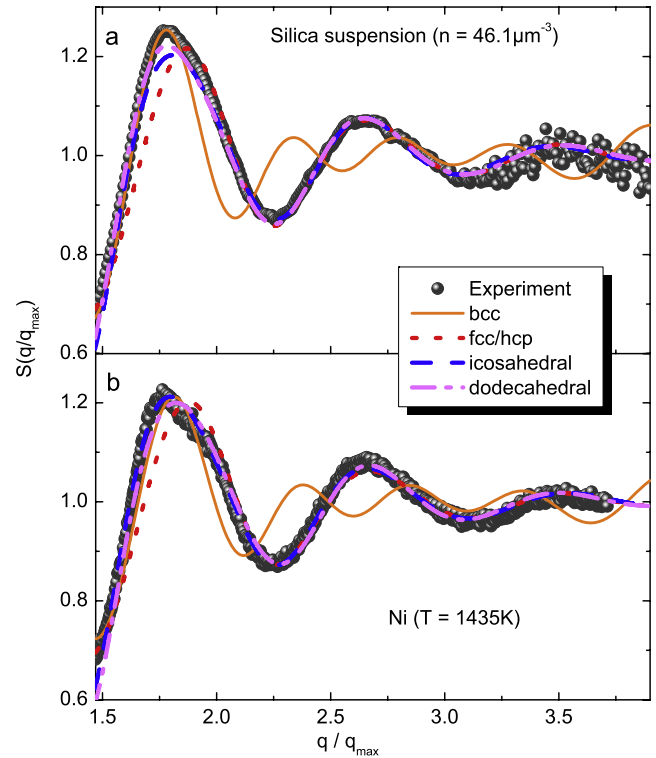


Figure 9. Structure factors $S(q/q_{\max})$ of a colloidal system in the metastable liquid state with $n = 46.1 \mu\text{m}^{-3}$ (a) and an undercooled melt of pure nickel at $T = 1435 \text{ K}$ corresponding to an undercooling $\Delta T = 291 \text{ K}$ (b); measured data are represented by symbols and results of simulations assuming a short-range order with different symmetries prevailing in the melt: bcc (brown curve), fcc and hcp (dashed red curve), icosahedral (dashed blue curve) and dodecahedral (solid pink curve).

clusters. The contributions from both these two different intra-cluster distances result in a total simulation curve including the asymmetric shape of large oscillations at about $q/q_{\max} = 1.8$. The asymmetry in $S(q/q_{\max})$ can be seen as an indication of the preference of an icosahedral short-range order [35].

The structure factor of the fluid phase is measured for a colloidal silica system (Si84) by USAXS at various states of metastability. The deviations from equilibrium for the colloidal suspension are determined by the chemical potential difference $\Delta\mu$ between the metastable fluid and the stable solid. The asymmetry in the second oscillation is most pronounced at a particle number density $n = 113 \mu\text{m}^{-3}$ corresponding to the largest metastability of $16\Delta\mu/k_{\text{B}}T$. With decreasing deviations from equilibrium the asymmetry becomes weaker. In the stable fluid phase the short-range order approaches a face centred cubic-like order [10]. This behaviour differs from the structure factors measured on liquid Ni [29]. Corresponding deviation from equilibrium is measured in metallic systems by the Gibbs free energy difference between liquid and solid, $\Delta G = G_{\text{liquid}} - G_{\text{solid}} \propto \Delta\mu$, which is estimated in the case of pure metals [1] by the linear approximation $\Delta G = \Delta S_{\text{f}}(T_{\text{L}} - T) = \Delta S_{\text{f}}\Delta T$ with ΔS_{f} the entropy of fusion, T_{L} the melting temperature of the respective metal and ΔT the undercooling. The measurements of the structure factor on pure Ni demonstrate that in contrast to the colloidal system

the asymmetry of the second oscillation survives even if the temperature is increased in the region of the stable liquid phase. The different behaviour of short-range order in the liquid phase of colloidal and metallic systems when crossing the boundary between metastable and stable liquid will be the subject of a forthcoming paper [36].

The comparison of measured structure factors of a colloidal system in the metastable liquid state and of undercooled liquid nickel and their analysis by the same approach for simulating structure factors yields strikingly similar results if scaled with the scattering vector corresponding to the nearest neighbour distance. In particular for both physically different systems an asymmetric shoulder in the second oscillation of $S(q/q_{\max})$ is observed which becomes more pronounced with increasing deviations from equilibrium. It is important to note that the formation of short-range order of five-fold symmetry is obviously a universal behaviour for metals as investigations on a series of different metallic materials reveal [30–39]. The interaction of particles in charged colloidal systems is described by the Debye–Hückel potential (cf. equation (4.1)), whereas atomic interaction in metallic systems are often described by using a Lennard-Jones potential:

$$\Phi_{\text{LJ}} = \left[\left(\frac{r_{\min}}{r} \right)^{12} - 2 \left(\frac{r_{\min}}{r} \right)^6 \right]. \quad (4.2)$$

Both, the Lennard-Jones potential and the Debye–Hückel potential have a repulsive term, which depends on the inter-particle distance and is considered to be soft in comparison to the potential of a hard sphere system. Both potentials differ in that an attractive term is missing in the Debye–Hückel potential. The experiments clearly show that both systems exhibit strikingly similar scattering patterns and hence structures. Within the present structural analysis, the liquid state of the charged silica colloid and of the pure metal prefer a dodecahedral short-range order of five-fold symmetry in particular if the liquid is far away from equilibrium. From this experimental finding one may conclude that a soft repulsive term in the particle interaction is a precondition for the formation of icosahedral short-range order in metastable liquids. This is supported by previous theoretical investigations [40, 41].

The present investigations confirm that the formation of short-range order of five-fold symmetry is occurring not only in melts of pure metals but also in charged colloidal suspensions. From this point of view charged colloidal suspensions may be considered as proper model systems for metals to study short-range order phenomena. So far Frank’s hypothesis is also applicable to charged colloidal suspensions provided that the metastable liquid state is considered.

5. Crystal nucleation in liquid state of colloidal suspensions

5.1. Determination of the nucleation rate from measured structure factors

Nucleation is the process initiating the crystallization process in a liquid environment. It preselects the crystallographic

phase stable or metastable. Detailed knowledge of crystal nucleation is of great importance to develop a quantitative understanding in the formation of various solid phases of different properties from the liquid state of matter. In metallic systems the formation of nuclei in undercooled melts is running very fast. The frequency of impingement of atoms from a liquid to a growing nucleus is very high and in the order of 10^{13} Hz. This makes it extremely difficult to observe directly nucleation processes in undercooled metallic melts [1]. Charged colloidal systems are frequently discussed as model systems to study nucleation phenomena. In contrast to atomic systems they provide a sufficiently long experimental timescale for investigations. This is due to the large size of their particles (hundreds of nm) and the Brownian nature of their motion. Therefore, time dependent investigations of nucleation processes are possible. Nucleation was observed *in situ* in three dimensional real space in colloidal hard sphere suspensions by applying confocal microscopy [42, 43].

Nucleation is characterized by the time dependent nucleation rate $J(t)$, which is defined by the number of nuclei appearing per unit volume and time. For determination of the nucleation rate, it is necessary to observe the evolution of the crystallites from the metastable fluid state into the stable solid state. This process can be analysed indirectly by scattering methods where the time dependent structure factor $S(q, t)$ is measured. The structure factor of the crystalline phase can be extracted following the method of Harland and van Megen [44]. The structure factor of the fluid phase, $S_f(q)$ has to be scaled so that the intensity at the minimum q' of the structure factor is equal to the intensity recorded for the following time scans $S(q', t) = \beta(t) \cdot S_f(q')$ with a scale factor $\beta(t)$ chosen at each time step. This scaling assumes that the fluid density and composition retain the same throughout the crystallization. The crystalline part of the structure factor is determined by subtracting the scaled fluid part from the measured structure factor

$$S_c(q, t) = S(q, t) - \beta(t) \cdot S_f(q), \quad (5.1)$$

where $\beta(t)$ is the time dependent scaling factor. This scaling assumes that the underlying structure factor of liquid will not change its shape during crystallization: the density and composition of the fluid retain the same throughout the crystallization. The resulting crystal structure factor $S_c(q, t)$ is used to determine the properties characterizing the crystallization kinetics. The integrated intensity is related to the crystallinity, $X(t)$, the peak position q_m to the lattice spacing of the crystals and the full width at half height of the peak to the average size of the crystallites, $\langle L(t) \rangle$.

The crystallinity, $X(t)$ (the fraction of the sample which is crystalline), is determined by integrating the structure factor over the area of the main Bragg reflection:

$$X(t) = c \int S_{\text{total}}(q, t) dq, \quad (5.2)$$

with normalization factor c . The lattice constant g of the crystal phase is calculated from the peak position q_{hkl}

$$g(t) = \frac{2\pi}{q_{hkl}(t)} \sqrt{h^2 + k^2 + l^2}, \quad (5.3)$$

where h, k, l are the Miller indices.

The average crystal size L is inverse to the full width at half height Δq following the Scherrer equation:

$$\langle L(t) \rangle = \frac{2\pi K}{\Delta q(t)}. \quad (5.4)$$

From these basic parameters, the number density of crystallites n_{xtal} and the nucleation rate density $J(t)$ can be determined. The number density of crystallites is deduced from

$$n_{xtal}(t) = \frac{X(t)}{\langle L^3(t) \rangle} = \frac{X(t)}{\alpha \langle L(t) \rangle^3} \quad (5.5)$$

with the parameter $\alpha \approx 1.25$ relating the average crystal size cubed [45]. The nucleation rate density is defined as the rate at which crystals appear in the liquid volume:

$$J(t) = \frac{1}{(1 - X(t))} \cdot \frac{d}{dt} \frac{X(t)}{\langle L^3(t) \rangle}. \quad (5.6)$$

This quantity represents the number of critical nuclei, which form inside a unit volume of the metastable liquid. The nucleation rate is normalized with respect to the remaining liquid volume, $1 - X(t)$.

Figure 10 illustrates the time dependent behaviour for the parameters extracted from the sequence of the time dependent structure factor measured: (a) crystallinity X , (b) average crystal size L , (c) crystallite density and (d) nucleation rate densities J .

The typical crystallization experiment in charged colloids shows a sigmoidal curve of crystallinity versus time as shown in figure 10(a). The curve exhibits initially a sharp increase of the crystallinity, which is attributed to nucleation and growth of crystals. Once the sample has reached the equilibrium state, this process decreases. The slow rise at long times is identified as the ripening or coarsening process where large crystals grow at the expense of smaller ones. The crystal of average size L grows to a size of approximately $1.1 \mu\text{m}$ and the nucleation rate density first increases from $J = 10^{17} \text{ m}^{-3} \text{ s}^{-1}$ by about one order of magnitude, achieves a maximum value at $J = 8 \times 10^{17} \text{ m}^{-3} \text{ s}^{-1}$ and decreases again. The parameters introduced are important to understand and to describe nucleation processes in colloids as well as in atomic or molecular systems. The time dependence of the nucleation parameters is not accessible in metallic systems with the exception of crystallization experiments of metallic glasses [46, 47]. In crystallization experiments of metallic glasses the time evolution of nucleation is controlled by the high viscosity of the deeply undercooled melt slightly above the glass transition temperature and, therefore, becomes very sluggish opposite to nucleation processes in melts undercooled below their melting temperature in a temperature range, where the viscosity is much smaller than in the region around the glass transition temperature.

5.2. Crystal nucleation in colloidal suspensions

Crystal nucleation is a thermally activated process with competing bulk and surface contributions to its energy balance. The nucleation rate is obtained by considering

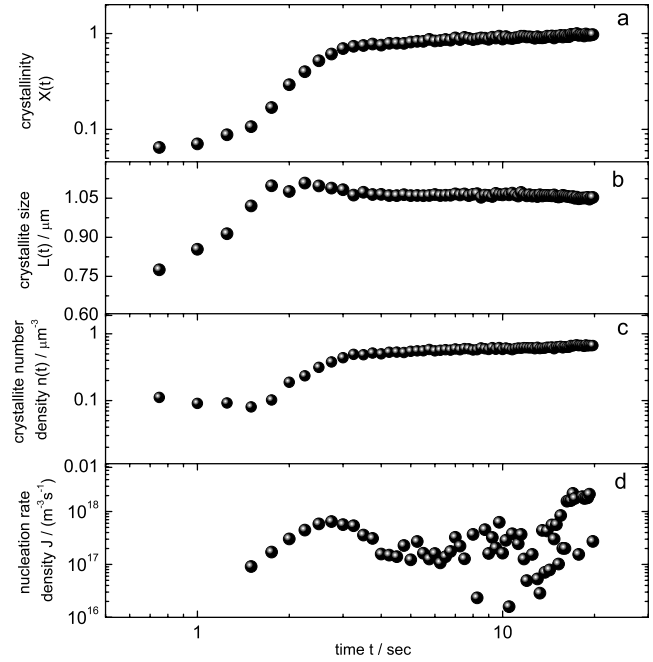


Figure 10. Time traces of extracted nucleation parameters from scattering data (a) crystalline volume fraction $X(t)$ or crystallinity, (b) average crystallite size $L(t)$, (c) crystallite number density $n(t)$, and (d) nucleation rate densities $J(t)$ exemplarily shown for a charged silica system with particles of size 77 nm and a particle number density $n = 224.7 \mu\text{m}^{-3}$.

the transition rates of elementary particles from the fluid to the growing nucleus and vice versa. By considering the Boltzmann distribution function for classical systems (no quantum physical processes) the nucleation rate density increases exponentially with increasing deviation from thermodynamic equilibrium. According to classical nucleation theory (CNT) [48] clusters of crystalline structure are formed in statistically independent events by stepwise addition of particles from the fluid, the formation of clusters of critical size is thermally activated across a barrier due to the interfacial energy between crystal nucleus and surrounding liquid, $\gamma > 0$. The nucleation barrier ΔG^* to form sphere-like nuclei of critical size of colloidal suspensions in the fluid state is given by

$$\Delta G^* = \frac{16\pi}{3} \cdot \frac{\gamma^3}{(n\Delta\mu)^2}, \quad (5.7)$$

where n is the particle number density and $\Delta\mu$ the difference of chemical potential between the solid and liquid state. For colloidal particles crossing the solid-liquid interface, the steady state nucleation rate, J_{ss} , is determined by

$$J_{ss} = J_o \exp\left(-\frac{\Delta G^*}{k_B T}\right), \quad (5.8)$$

where J_o is the kinetic prefactor that depends on the diffusion coefficient and the number of potential nucleation sides. Despite its simplicity, the CNT is widely used to parameterize nucleation both in metallic undercooled melts [1, 49] and colloidal systems as well [19, 50–52]. While in metallic systems the interaction potential acting on the individual

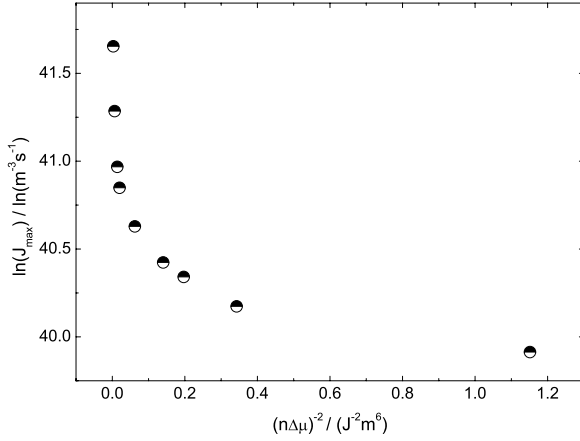


Figure 11. Arrhenius plot of the nucleation rate densities at maximum interaction J_{\max} versus $(n\Delta\mu)^{-2}$ measured for a silica suspension. The plot shows that with increasing metastability the logarithm of the nucleation rate density deviates from a linear decay. This behaviour is understood by a dependence of both the interfacial energy γ and the kinetic prefactor J_o on the particle number density n . The interfacial energy and the kinetic prefactor are determined by the local slope and the intercept with the ordinate at each data point as a function of n , respectively.

atoms is fixed, the interaction potential in charged colloidal suspensions depends on the particle number density. This raises the question whether CNT is available for charged colloidal suspension. So far, experimental data of nucleation in charged colloidal systems are rare. The following part will address this issue. The nucleation rate densities as determined from the USAXS measurements will be analysed as a function of the particle number density within CNT using the expression for steady state nucleation rate J_{ss}

$$J_{ss} = 12 \left(\frac{4}{3} \right)^{2/3} \pi^{-1/3} \sqrt{\frac{\gamma}{k_B T}} \cdot \frac{D}{d_{NN}^2} n^{2/3} \cdot \exp\left(-\frac{\Delta G^*}{k_B T}\right). \quad (5.9)$$

D denotes the long time self-diffusion coefficient in fluid phase and d_{NN} the next-nearest neighbour distance. Equation (5.9) takes into account that in monodisperse charged colloidal systems under fully deionized conditions, the particle number density of the crystal and the fluid are equal [50]. From equation (5.9) the unknown parameter of the interfacial energy γ are determined provided data for the steady state nucleation rate and the diffusion coefficient are available. Following Wette and Schöpe [50] there is, however, another method to determine the interfacial energy from measurements of the steady state nucleation rate without the need of data of the diffusion coefficient to be available. This method does not use the representation of the kinetic prefactor J_o according to equation (5.8) and, thus, avoids the need of the knowledge of the diffusion coefficient.

Using the logarithm of equation (5.8) yields

$$\ln(J_{ss}) = \ln(J_o) - \frac{16\pi\gamma^3}{3k_B T} \cdot \frac{1}{(n\Delta\mu)^2}. \quad (5.10)$$

For a particle number density independent interfacial free energy and kinetic prefactor, a straight line in a diagram of

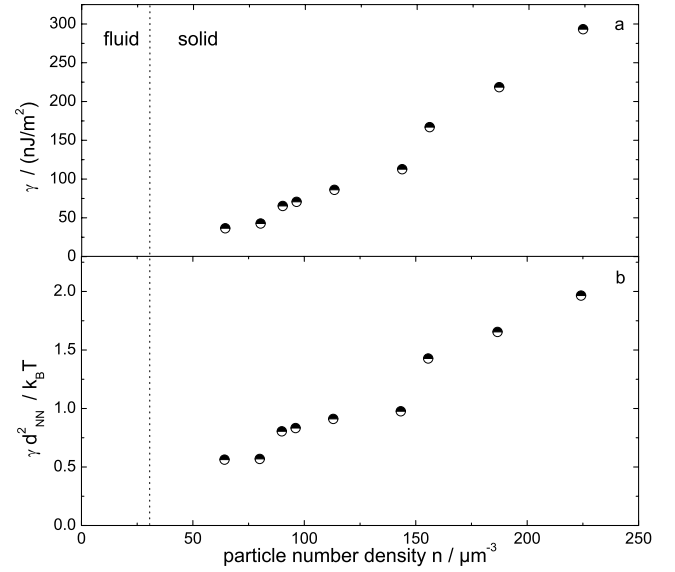


Figure 12. Absolute (a) and reduced (b) interfacial energy in dependence of particle number density determined from measurements of Si77 colloidal system showing a nearly linear increase.

$\ln(J_{ss})$ versus $(n\Delta\mu)^{-2}$ with the slope $m = (16\pi/3k_B T)\gamma^3$ according to equation (5.10) is expected. In metals, the interaction potential is fixed, a linear relation between $\ln(J_{ss})$ and $(n\Delta\mu)^{-2}$ should hold. In fact, this has been experimentally observed by studies of nucleation in undercooled melts of the glass forming alloy $\text{Pd}_{40}\text{Ni}_{40}\text{P}_{20}$ [53]. In contrast to metals, the interaction of particles in charged colloidal suspensions depend on the particle number density and the relation between $\ln(J_{ss})$ and $(n\Delta\mu)^{-2}$ shall deviate from a straight line.

The nucleation rate density is inferred from the measured nucleation rate densities as the value at the maximum of the time dependent nucleation rate, J_{\max} , according to figure 10(d), assuming that $J_{\max} = J_{ss}$. Figure 11 shows a so-called Arrhenius plot of the data obtained by the USAXS measurements for silica suspension Si77 that clearly shows a non-linear behaviour of $\ln(J_{\max})$ versus $(n\Delta\mu)^{-2}$.

The non-constant slope in the Arrhenius plot demonstrates that the interfacial energy as well as the prefactor are a function of the particle number density: $m(n)$ and $J_o(n)$. Considering the particle number density dependence of the interfacial energy and the kinetic prefactor, the local slope of $\ln(J_{\max})$ versus $(n\Delta\mu)^{-2}$ is calculated using $m(n) = \Delta \ln(J_{\max}) / \Delta (n\Delta\mu)^{-2}$. The interfacial energy $\gamma(n)$ depending on the particle number density n is then given by

$$\gamma(n) = \left[\frac{3m(n)k_B T}{16\pi} \right]^{1/3}. \quad (5.11)$$

Figure 12(a), upper part, presents the data of the interfacial energy $\gamma(n)$ as determined by the graphical method. In order to compare the results of interfacial energy with atomic systems as well as to other colloidal systems and results of simulations, figure 12(b), lower part, shows the reduced interfacial energy $\gamma^* = \gamma d_{NN}^2 / k_B T$. The reduced interfacial

energy is scaled with the next-neighbour distance instead of the particle diameter d as usual in hard sphere systems, because charged particles are not close packed. A roughly linear increase of γ^* with n is observed. This result is different to hard sphere systems where a constant value $\gamma d^2 = 0.55k_B T$ is predicted [54].

The interfacial free energy γ increases from 30 nJ m^{-2} up to about 300 nJ m^{-2} with increasing n . The kinetic prefactor $J_o(n)$ can be determined from the intercepts with the ordinate for each data point concerning the respective values of the particle number density.

A method to determine the interfacial energy and the kinetic prefactor from measured time dependent nucleation rate densities is the usage of equation (5.9) provided by CNT. The calculations require the knowledge of the long time self-diffusion coefficient D as a function of n . In this case, it is possible to solve equation (5.9) for γ as the only remaining unknown parameter. The estimate of the diffusion coefficient appears to be quite difficult and remains dependent on assumptions as pointed out in the literature [55]. Because of the uncertainty in the determination of the diffusion coefficient we do not make use of this method to infer the interfacial energy from solving equation (5.9) with measured nucleation rate data.

In systems with high relaxation rates the formation of clusters within the liquid follows instantaneously any change of state of the systems. Under such circumstances nucleation is considered as taking place under steady state conditions. Such conditions are certainly present in liquid metals in a temperature range around the melting temperature in which atomic relaxation takes place very rapidly because of very high self-diffusion coefficients in the liquid state. In monoatomic metallic systems atomic movement in the liquid is even considered to be collision limited i.e. the frequency in the order of the Debye frequency will set the limit for the frequency of atomic place changes [56]. Even in melts of alloys, in which atomic movement is diffusion controlled atomic replacement in liquid state is occurring rapidly compared to the timescale of changes in their state for instance during rapid cooling [57]. On the other hand, during crystallization of metallic glasses around the glass transition temperature at which the viscosity is very high in the order of 10^{13} P compared to about 10^{-2} P at the melting temperature of pure metals, transient effects become important in crystal nucleation processes in metallic glasses [58].

In colloidal suspensions movement of the particles in the liquid state is controlled by Brownian motion. Compared with movements of atoms in liquid metals, Brownian motion is very sluggish. Therefore, one would expect that transient effects in crystallization of colloids could be of importance. In the present work, we make an attempt to consider transient effects in the nucleation behaviour of silica suspensions. To do so, the experimentally determined time dependent nucleation rate densities were evaluated applying the theory of transient nucleation by Kashchiev [59]. Accordingly, the time dependent nucleation rate is given by

$$J(t) = J_{ss} \left[1 + 2 \sum_{m=1}^{\infty} (-1)^m \cdot \exp\left(-\frac{m^2 t}{t_i}\right) \right], \quad (5.12)$$

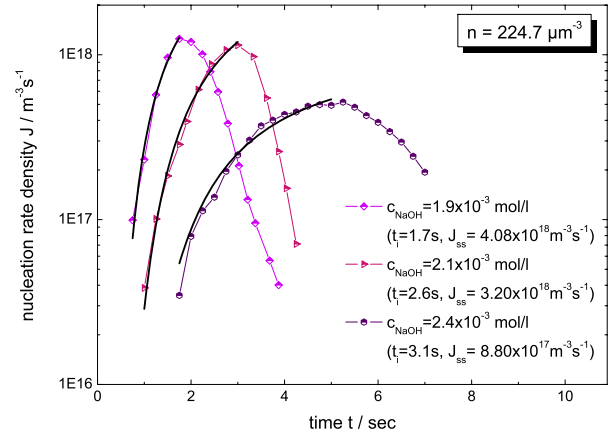


Figure 13. Steady state nucleation rate densities J_{ss} and the corresponding induction time t_i obtained by fitting the measured time dependent nucleation rate density $J(t)$ according to the expression developed by Kashchiev for transient nucleation.

where J_{ss} denotes the steady state nucleation rate and t_i the induction time given by

$$t_i = \frac{\gamma d_{NN}^2 k_B T}{(3/8)(4/3)^{2/3} \pi^{5/3} D n^{2/3} (\Delta\mu)^2}. \quad (5.13)$$

The induction time determines the time of the delay for the onset of crystal nucleation in experiments of rapid changes of the states. There are two unknown parameters in equation (5.12). That is the long time self-diffusion coefficient D and the interfacial energy γ . The consideration of transient effects in nucleation of colloidal suspensions offers the possibility to determine independently the self-diffusion coefficient D from the measured transient time according to equation (5.13). In colloidal suspensions, the self-diffusion coefficient will depend on the particle number density n , $D(n)$. Thus, the interfacial energy, γ , can be determined from measurements of nucleation rates provided homogeneous nucleation dominates. Figure 13 shows measured nucleation rates for silica colloidal suspensions at fixed particle number density $n = 224.7 \mu\text{m}^{-3}$ at three different salty concentrations.

No solution of equations (5.9) and (5.13) exists for the nucleation rates $J(t)$ shown in figure 13. According to figure 13 for all investigated silica colloidal suspension the nucleation rate steeply rises, passes through a maximum and rapidly falls at large times. The nucleation rate density does not approach a stationary state where a dynamic equilibrium is achieved in the formation of nuclei per volume and time unit. We assume that the nucleation rate collapses without achieving the steady state nucleation rate [51, 52]. This assumption is supported by a comparison of the results of silica suspension of the present work with previous investigations of nucleation behaviour in polystyrene colloidal suspensions. Figure 14 displays the time dependent nucleation rates of a completely deionized polystyrene colloidal suspension (PnBAPS68) with particles with a size of $68 \text{ nm} \pm 3 \text{ nm}$ which are dispersed in water. These particles carry strongly acidic sulfate groups on their surface, which are completely dissociated in an aqueous environment leading to a maximum effective charge. Here

the particle interaction is controlled by the particle number density, which was slightly increased from $18 \mu\text{m}^{-3}$ up to $20 \mu\text{m}^{-3}$. Results obtained by measurements of three different colloidal suspensions with various particle number densities are shown [17]. A plateau like levelling off after the steep rise in the beginning is obvious in particular for colloidal suspensions with small particle concentrations. That is different to the behaviour of the time dependent nucleation rates measured on the silica systems. Opposite to the nucleation rates $J(t)$ measured for silica colloidal systems, equations (5.9) and (5.13) can be solved for the data of $J(t)$ measured for the polystyrene suspension. The steady state nucleation rates as inferred from fitting the measured time dependent nucleation rates result in values, which are by ten orders of magnitude smaller than the kinetic nucleation rate J_0 . That is reasonable within nucleation theory with respect to the ratio of J_0 and J_{ss} .

6. Interfacial energy and Turnbull plots of colloids and metals

6.1. Metallic systems

The solid–liquid interfacial energy is of importance to describe crystallization in liquid systems. Concerning metals and alloys, the interfacial energy between the solid and liquid phase is measured by the so-called grain boundary method. Here, the grain boundary angles of a fluid groove formed at a solid–liquid interface between two neighbouring grains is measured. Provided, data are available for the grain boundary interfacial energy between the two neighbouring grains, the interfacial energy between solid and liquid can be determined [60]. However, such measurements are restricted to the determination of the solid–liquid interface under the conditions of thermodynamic equilibrium. Since nucleation requires an undercooling to create a driving force for overcoming the activation threshold to form nuclei of critical size, the equilibrium values determined by the grain boundary method are of limiting applicability. Values for the interfacial energy between a solid nucleus within an undercooled melt have been indirectly investigated by measurements of maximum undercoolability. Under the assumption of homogeneous nucleation the interfacial energy is inferred from the analysis of experimental results of maximum undercooling within the classical nucleation theory. Results obtained by the two different methods are available for pure bismuth. The application of the grain boundary method yields $\gamma = 61.3 \times 10^{-3} \text{ J m}^{-2}$ compared to $\gamma = 54.4 \times 10^{-3} \text{ J m}^{-2}$ obtained from measurements of maximum undercooling [61]. Apparently, both values differ by about 15% leaving a large uncertainty in the knowledge of the solid–liquid interfacial energy.

The first systematic investigations of nucleation behaviour for a variety of different metals were conducted by Turnbull in the 1950s [62, 63]. He developed the emulsion technique. The macroscopic melt was subdivided into many small droplets to isolate heterogeneous nucleation sites in a minority of the droplets. Later on, this technique was refined by dispersing

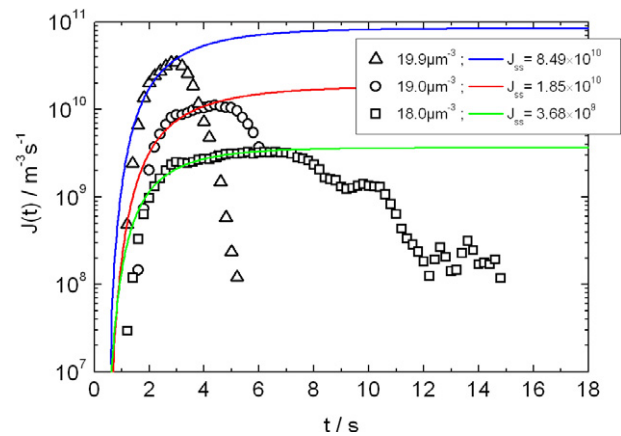


Figure 14. Time dependent nucleation rate $J(t)$ as measured on polystyrene colloidal suspensions PnBAPS68 at various particle number densities $n = 19.9 \mu\text{m}^{-3}$ (blue), $n = 19.0 \mu\text{m}^{-3}$ (red), and $n = 18.0 \mu\text{m}^{-3}$ (green) [17].

the droplets in an emulsion of oil or aqueous solutions in the presence of surfactants to stabilize the droplets of $10\text{--}100 \mu\text{m}$ in size and to passivate heterogeneous nucleation sites on the surface of the droplets. In such a way Turnbull was successful in undercooling the liquid droplets to values of about 20% of the melting temperature of the respective metals. Because of this unique behaviour observed for a great variety of different metallic elements he assumed that the limiting case of homogeneous nucleation was achieved. The interface energy was then determined by analysing the values of maximum undercooling within homogeneous nucleation theory.

In order to compare the results of interfacial energies for various systems, Turnbull [34] defined a gram-atomic or molar interfacial energy γ^* of a one atom thick interface. Based upon the experimental results of maximum undercooling observed in the droplet dispersion experiments, Turnbull proposed an empirical relation between the interfacial energy γ^* and the latent heat of fusion per gram atom, ΔH_f :

$$\gamma^* = \alpha \rho^{-2/3} \Delta H_f \quad (6.1)$$

with ρ the number density of the solid and α the dimensionless solid–liquid interfacial energy or the Turnbull coefficient. The results by Turnbull are shown in figure 15 (top left). Turnbull obtained a value of $\alpha = 0.45$ for most of the pure metals especially of those of them, which form close packed structures such as fcc or hcp structures in the solid state. For non-metallic systems he found $\alpha = 0.32$. Although heterogeneous nucleation is suppressed by a substantial amount, the droplet dispersion technique was not able to completely avoid heterogeneous nucleation. More advanced methods such as containerless processing under high purity environment conditions have demonstrated that even in macroscopic melts in size of several mm undercoolings were measured exceeding the previous values by Turnbull [1]. Therefore, the values of the reduced interfacial energies obtained by Turnbull are assumed to give a lower limit for the interfacial energy.

More recently, comparative undercooling experiments on bulk zirconium melts were performed using electromagnetic

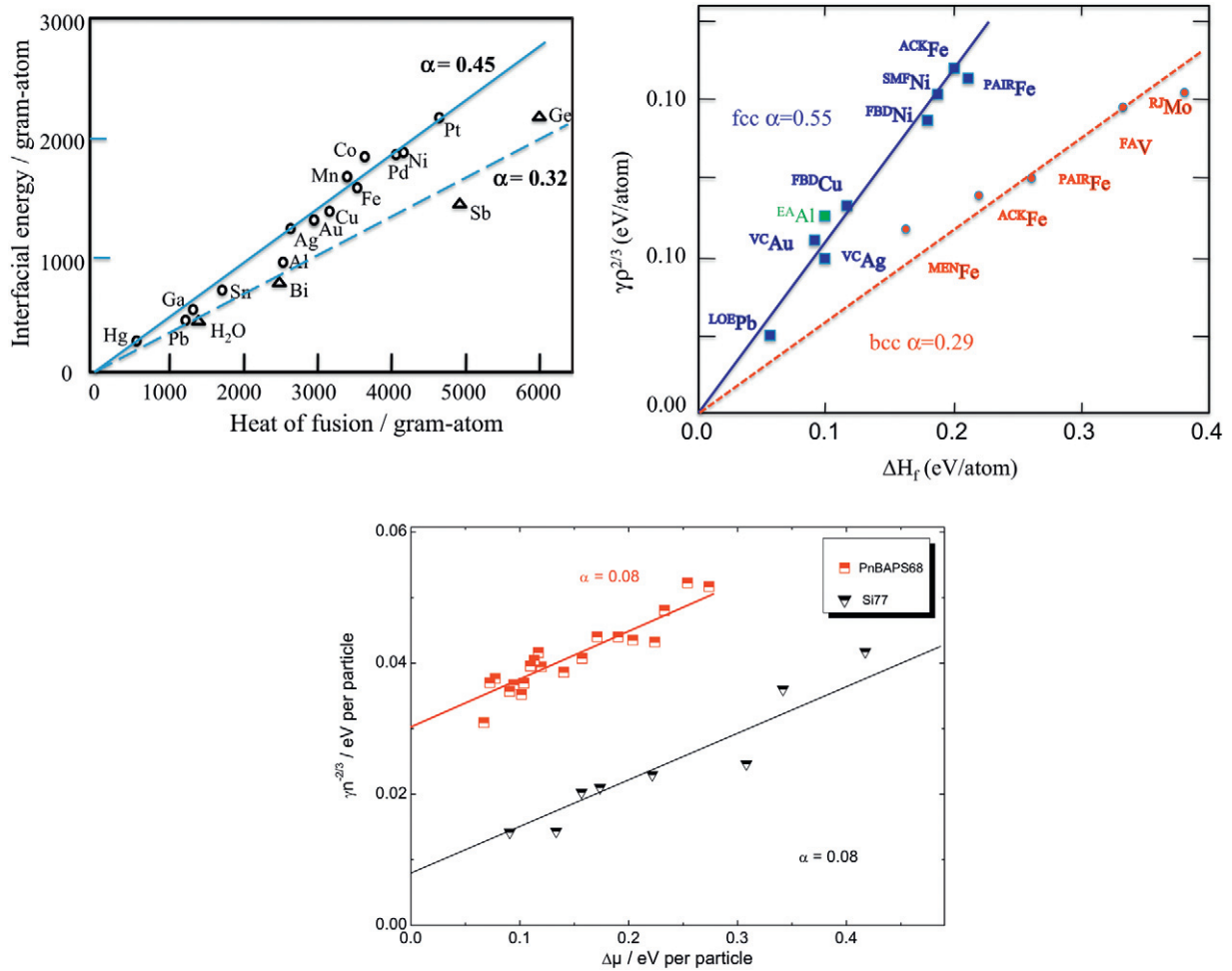


Figure 15. (Top left) Gram-atomic interfacial energy as a function of the gram-atomic heat of fusion for various metallic and non-metallic substances [34], (top right) results of simulations for metals, the labels on each data point refer to the specific form of the EAM potential used in the simulations, see [75] and references therein, (bottom right) results of measurements on colloidal suspensions, the triangles (down) give results of silica suspensions Si77 [10] and the squares refer to polystyrene PnBAPS68 [7]. The lines are determined by the graphical method (see section 5.2).

and electrostatic levitation techniques. By statistical analysis of about 100 subsequent undercooling and crystallization experiments values for both the activation energy ΔG^* to form nuclei of critical size and the prefactor in the nucleation rate according to equation (5.8) were obtained. While the analysis of the experiments in the electromagnetic levitator reveal heterogeneous nucleation despite the large undercoolings in average of 330 K obtained, the analysis of the experiments using the electrostatic levitator leads to enhanced undercooling values in average of 370 K and the conclusion that the limiting case of homogeneous nucleation may be approached. The larger undercoolings observed in the electrostatic levitation experiments were attributed to the fact that the liquid drop was processed under ultra-high vacuum (UHV) conditions whereas the electromagnetic levitation experiments were conducted under a helium environmental gas atmosphere in purity not comparable to the UHV condition [64]. From the undercooling experiments in the electrostatic levitator values for the dimensionless interfacial energy were inferred. The data are given in table 2 together with other results.

6.2. Results of modelling and simulations

There are many attempts to develop models for computing the interfacial energy analytically. The model frequently used to evaluate the interfacial energy is the negentropic model by Spaepen [65, 66]. It treats a system of densest packing of hard spheres and assumes that only configurational entropy contributes to the interfacial energy. Vibrational contributions to the entropy and enthalpic contributions are neglected. In order to determine the configurational entropy the interface is structurally formed according to the criteria of (i) tetrahedral short-range order is preferred, (ii) octahedral short-range order is forbidden, and (iii) the density is maximized. In such a way, Spaepen defined a dimensionless solid-liquid interfacial energy as

$$\alpha := \frac{\gamma(T_m)}{\Delta H_f}, \tag{6.2}$$

with ΔH_f the enthalpy of fusion. Analytical solutions for bcc structure of $\alpha = 0.70$ [67] and fcc structure of $\alpha = 0.85$ [65, 66] were reported. Later, the model was extended,

which allows for numerical determination of solid–liquid interfacial energies even for complex structured alloys [68].

In other approaches, γ is determined by molecular dynamics simulations or in the framework of density functional theory (DFT) [69]. For the investigations it is assumed that the density $\rho_S(\mathbf{r})$ of the solid phase is a function of the position \mathbf{r} and shows the symmetry of the solid. The density ρ_L of the liquid is treated as being constant. Within the interface region the density $\rho(\mathbf{r})$ changes continuously from the density value $\rho_S(\mathbf{r})$ of the bulk solid phase to the density of the liquid, ρ_L . Then, $\rho(\mathbf{r})$ is obtained by minimization of the function

$$\Delta\Phi = \Phi(\rho(\mathbf{r})) - \Phi_L = F(\rho(\mathbf{r})) - \mu_L \int \rho(\mathbf{r}) d\mathbf{r} + pV, \quad (6.3)$$

where Φ is the grand potential, Φ_L the grand potential of the liquid, μ_L the chemical potential of the liquid, p the pressure and V the volume [70]. If O denotes the surface of the phase boundary, the interfacial energy between solid and liquid will be

$$\gamma = \frac{\Delta\Phi}{O}. \quad (6.4)$$

The function $\rho(\mathbf{r})$ that minimizes the free energy difference ΔF between solid and liquid is determined by variation techniques. Information on the short-range order in the liquid phase enters into density functional theory via correlation functions. The correlation functions are often estimated in the framework of the Percus–Yevick approximation [71]. Depending on the atomic interaction potentials the various density functional calculations deliver substantially different results on the solid–liquid energy.

Molecular dynamics simulations of the interface between solid and liquid enable to treat aspects related to the short-range order both in the liquid and solid phase when estimating the interfacial energy. Similar to DFT, the results of the molecular dynamics simulations are strongly dependent on the choice of the interaction potentials, leading to a broad spread of values for the interfacial energy [72–74]. This demonstrates the importance of investigating systems with well-defined potentials, which can even be tuned in using charged colloidal systems as model systems for direct experimental investigations.

Hoyt *et al* [75] have compared results of theoretical investigations and computer simulations with experimental data of the dimensionless solid–liquid interface. Figure 15 (top right) shows the results of modelling of the dimensionless interfacial energy for different metals forming either fcc or bcc structure in the solid state. This diagram reveals that the dimensionless interfacial energy α depends on the structure of the nucleus formed in the undercooled melt. It is found that for fcc $\alpha = 0.55$ and for bcc $\alpha = 0.29$, respectively. The interfacial energy is computed by the capillary fluctuation method. The labels for each data point include the embedded atom method (EAM) potential used in the simulations. Apparently, in qualitative agreement with the negentropic model by Spaepen, the computed interfacial energies for bcc forming metals is systematically smaller than that of fcc forming metals. However, the numerical values for the dimensionless interfacial energies differ between

the predictions of the negentropic model and the computer simulations. The value of the dimensionless interfacial energy deduced from the statistical analysis of undercooling experiments on zirconium droplets in the electrostatic levitator is much closer to the values predicted by the negentropic model by Spaepen than the values obtained from the simulation work. Also the results obtained from undercooling investigations of other metals lead to the same conclusion. These results suggest that the computer simulations lead to a systematic underestimation of the solid–liquid interfacial energies [64].

6.3. Colloidal suspensions

Concerning colloidal suspensions the heat of fusion released during crystallization of the liquid phase is not known so far. It is expected that it will be much smaller than the heat of fusion of metals since the number of particles in colloidal systems is much smaller than the number of atoms in metallic systems. It may be possible to determine the heat of fusion in colloidal suspensions by micro-calorimetry. However, up to now any experimental investigations for determining the heat of fusion in colloidal suspension are lacking. For a first approach, one may use the difference of the chemical potential in order to construct an analogue of the Turnbull plot for colloidal systems. The chemical potential difference $\Delta\mu$ determined for colloidal suspensions corresponds to the difference of the free enthalpy ΔG for atomic systems. ΔG contains both the heat of fusion and the difference of enthalpic and entropic contributions between solid and liquid. In this case, the Turnbull expression for colloidal systems may be written as

$$\gamma = \alpha \cdot \Delta\mu \cdot n^{2/3} \quad (6.5)$$

with α the Turnbull coefficient. Figure 15 (bottom) shows the Turnbull plot measured in colloidal systems.

The squares in figure 15 (bottom) correspond to the reduced interfacial energy of the charge stabilized colloidal suspension PnBAPS68 [7] and the triangles represent equivalent results for silica suspension Si77 [10].

Comparing all diagrams of figure 15 qualitatively, the same behaviour is found. This means that the reduced interfacial energy increases with the heat of fusion as experimentally investigated for various metals and some non-metallic systems (figure 15 top left), studied by computer simulations (figure 15 top right), and as measured for colloidal systems the reduced interfacial energy increases with the difference of chemical potential. However, there is one important difference between measurements on metals and computer simulation results on the one hand and the experimental findings obtained for colloidal systems on the other hand. In the case of colloidal systems there is an offset of lines through the data points. This makes no physical sense, since the interfacial energy is expected to be zero at the equilibrium point, $\Delta\mu = 0$. This may be a consequence that the heat of fusion during crystallization of liquid colloidal systems has not yet been individually determined.

The different results between both colloidal systems among themselves evaluated by explicit calculations within the framework of classical nucleation theory also reflect the

Table 1. Experimental results of the dimensionless solid–liquid interfacial energy (Turnbull coefficient α). The results obtained from experimental investigations of maximum undercoolability give a lower limit of the reduced interfacial energy since the assumption of homogeneous nucleation being necessary for the analysis within classical nucleation theory with respect to the determination of the interfacial energy may be not justified. In case of colloidal systems homogeneous nucleation is discriminated unambiguously from heterogeneous nucleation, but the numerical values obtained for the Turnbull coefficients are much smaller compared with the corresponding figures of metals. This may reflect the difference in bonding of elementary particles between hard and soft matter materials.

System	Method	Stable phase	Turnbull coefficient α	Reference
Si77	Graphical	bcc	0.08	[10]
PnBAPS68	Graphical	bcc	0.08	
Cu	Melt fluxing	fcc	0.80	[80]
Co	Melt fluxing	fcc	0.67	[81]
Fe	Electromagnetic levitation	bcc	0.60	[1]
Zr	Electrostatic levitation	hcp	0.61	[64]
Co ₅₀ Pd ₅₀	Electromagnetic levitation	fcc	0.57	[81]
Co ₇₀ Pd ₃₀			0.55	

difficult interpretation of interfacial energies. The main reason for the discrepancy of the results can be possibly attributed to transient effects, which are not taken into consideration in the investigations of the PnBAPS68 system. Also, the polydispersity of colloidal systems may contribute to the difference of the dimensionless interfacial energies of both colloidal systems. The polydispersity for the PnBAPS68 system is about 2%, while it is slightly higher in the silica system of about 8%. A significant influence of polydispersity on the nucleation behaviour in hard sphere systems was recently reported [76]. Charged colloids are known to be less sensitive on polydispersity concerning their interaction or structural behaviour, but it might play a more significant role in forming a microscopic interface between a metastable fluid and stable solid.

Both colloidal systems, PnBAPS68 and Si77, crystallize in a bcc structure and are expected to form a similar short-range order in the state of metastable liquid phase. Detailed investigations of the short-range order in the metastable fluid state of the Si77 suspension reveal an icosahedral short-range order. Considering these properties within the negentropic model of Spaepen, a Turnbull coefficient $\alpha = 0.70$ is expected for both colloidal suspensions. This is in discrepancy with the experimental findings on the colloidal suspensions, which indicate a much smaller dimensionless interfacial energy than predicted by the negentropic model.

Using free energy calculations on small crystalline clusters, Cacciuto *et al* estimated the interfacial energy for the solid–liquid equimolar interface of a system of hard sphere colloids [77]. The dependence of γ on the radius of a nucleus was determined. An extrapolation to infinite radius yields a value for a planar interface as $\gamma(r \Rightarrow \infty) = 0.616$. He considers the dependence of the interfacial energy on the degree of metastability. The simulations suggest that γ

Table 2. Results of calculations and computer simulations for the Turnbull coefficient for crystals with fcc and bcc structure. The abbreviations denote: dense packing of hard spheres (DPHS), density functional theory (DFT), molecular dynamics simulations (MD). Different interaction potentials are assumed: hard sphere (HS), Lennard-Jones (LJ), adhesive sphere (AS) and embedded atom method (EAM).

Authors	Method	Potential	α (fcc)	α (bcc)
Spaepen [65, 66]	DPHS	HS	0.85	0.70
McMullen and Oxtoby [82]	DFT	HS	0.87	
Broughton and Gilmer [83]	MD	LJ	0.36	
Curtin [84]	DFT	LJ	0.45	
Marr and Gast [85]	DFT	HS	0.43	
Ohnesorge <i>et al</i> [86]	DFT	AS	0.48	0.48
		HS	0.44	0.46
Davidchack and Laird [73]	DFT	LJ	0.18	
		HS	0.24	
Davidchack and Laird [73]	MD	HS	0.48	
Hoyt <i>et al</i> [74, 87]	MD	EAM (Ni, Cu, Al, Au, Pb)	0.55	
		EAM (Fe)		0.32
		EAM (Fe, V, Mo)		0.29

associated with the equimolar surface is fairly insensitive to changes in metastability. This result obviously does not apply to charge stabilized colloidal systems. Granasy *et al* developed a phase field theory for the solid–liquid interfacial energy under non-equilibrium conditions of binary systems [78]. The results of undercooling experiments on Ni–Cu melts over the entire concentration range [79] were re-evaluated within this model. For this analysis a Turnbull coefficient $\alpha = 0.6$ was assumed that is close to the results of molecular dynamics simulation by Hoyt [74]. A quantitative agreement with the experimental results was achieved assuming homogeneous nucleation. However, recently an undercooling value for pure Cu was reported from melt-fluxing experiments to be 352 K [80]. That is more than the phase field model for nucleation by Granasy *et al* predicts for the limiting case of homogeneous nucleation for copper. Also this comparison suggests that simulations often lead to an underestimation of the dimensionless interfacial energy. But the Turnbull coefficients as investigated for metals from both experimental and theoretical sides are much higher than the Turnbull coefficients obtained from investigations on colloidal systems. Such a large difference in the dimensionless interfacial energy between atomic and colloidal suspensions may reflect the different bonding situations in hard matter and soft matter materials. Nevertheless, it will be interesting to investigate whether colloidal systems will show qualitatively the same dependence of the interfacial energy on the structure of a crystal nucleus as predicted by the negentropic model [65, 67] and computer simulations [75] and experimentally tested by levitation undercooling experiments on metals and alloys [1].

Results of experiments to determine the Turnbull coefficient for metals and for colloidal systems are compiled in table 1, while table 2 gives equivalent results obtained from theoretical modelling and computer simulations.

7. Summary

We have investigated colloidal systems and their potentials as model systems to understand phenomena of crystallization in metallic systems, the establishment of short-range order in the metastable liquid state, phase behaviour and crystal nucleation. In particular, the crystallization of metals and its understanding is essential in materials production. However, some important parameters being of essential importance to describe crystallization and solidification as e.g. the solid–liquid interfacial energy are concealed in metals because they are non-transparent for light of optical wavelength and atomic relaxation processes take place at very high frequency in the order of the Debye frequency of 10^{13} Hz. For two decades it has been well known that colloidal suspensions behave analogous to metals with respect to the formation of ordered crystalline structure and even disordered amorphous solid phases. Colloidal suspensions differ from atomic systems in that the particles dissolved in a carrier liquid medium are orders of magnitude larger than atoms and their structural relaxation behaviour behaves much more sluggish than atomic systems. The particle–particle distance is ranging from some tens of nanometres up to a few micrometres and they are transparent for optical light in particular at small particle number densities. These properties make colloids interesting for usage as model systems to understand phenomena in crystallization of metallic systems by simple optical investigations. Moreover, in contrast to metallic systems with fixed atomic interaction potential, charged colloidal suspension offers the benefit of being able to tune the interaction potential of the elementary particles.

In the present work, we have investigated silica suspensions consisting of silica particles with average sizes of 77 nm and 84 nm, respectively, dispersed in water of high purity. Light scattering and ultra-small angle x-ray scattering using high intensity synchrotron radiation (USAXS) at HASYLAB in Hamburg have been applied to study short-range order phenomena in the metastable liquid state, to determine the phase diagram of silica colloidal suspensions and measure nucleation rate densities as a function of particle number density in a wide range even in the regime of high particle number density at which the systems become non-transparent, but in particular the silica suspensions are very suitable for USAXS measurements because of their contrast in x-ray measurements. The results obtained from the investigations of charged colloidal suspensions are discussed in relation to the corresponding behaviour of metallic systems in order to test them as model systems for understanding crystallization of metals.

The phase behaviour was studied leading to the construction of a phase diagram, in which the regions of existence of the liquid and solid bcc phase are shown in dependence on the particle number densities and the concentration of NaOH. The addition of NaOH leads first to a charging up of the silica particles passes through a maximum of interaction at which the effective charge of the particles is determined by measurements of the shear modulus. At further increasing the NaOH concentration a screening effect

leads to a decrease of the particle–particle interaction. At particle number densities larger than $n = 18 \mu\text{m}^{-3}$ a re-entrant phase behaviour is observed. At small NaOH concentration the system is in the stable disordered liquid state. With increasing salty concentration the system enters the region of stable bcc solid before it re-melts at further increasing NaOH concentration. It is worth emphasizing that the re-entrant phase behaviour is well known for a spectrum of physically different systems including formation of refined microstructures in metals and alloys and with respect to transitions of disordered to ordered and to disordered magnetic phases in some magnetic alloys.

Measurements of the structure factor by USAXS on silica colloidal suspensions shear melted allow the short-range order in the fluid state far from the thermodynamic equilibrium to be determined. The measured structure factor was analysed within a simple model that allows the determination of the dominating structural units. The same model was previously applied to analyse the structure factor of undercooled melts measured by elastic neutron scattering. The comparison of the measured structure factors of monodisperse colloidal suspension and pure metal leads to the conclusion that in both physically different systems an icosahedral and dodecahedral short-range order prevails. Such a short-range order with five-fold symmetry in metastable liquid metals was postulated by Frank 60 years ago to explain the undercoolability of metals.

The USAXS measurements allow for the determination of nucleation rate densities. A great advantage of colloidal suspensions compared with metallic systems is that homogeneous and heterogeneous nucleation can be unambiguously discriminated. This offers the potential to infer important parameters for crystallization from measurements of homogeneous nucleation rates in colloidal suspensions such as the interfacial energy. The results of such measurements were compared with predictions of theories, modelling and computer simulations. In metals, high interfacial energies are determined sometimes larger than the results predicted by computer simulations. In the case of colloidal suspensions the interfacial energies are much smaller than in metals. An open issue in the evaluation of nucleation rates in colloidal systems is the influence of transient effects in crystal nucleation in particular in systems of high particle number density. On the one hand, transient effects are expected in systems with sluggish relaxation behaviour as present in colloidal suspensions with respect to typical timescales of changes of state during experiments. On the other hand, the application of models of transient nucleation developed and applied for the analysis of nucleation studies of metals lead sometimes to non-solvable equations for measured nucleation rates. Another challenge for future studies on colloidal systems with respect to using them as model systems for metals concern colloidal suspensions of mixtures of particles of different size groups. In such systems a phase diagram may be constructed in some analogy to solid solutions, eutectics and intermetallics for metallic systems. Such investigations are currently the subject of research for the authors of this review.

Acknowledgments

The authors are very much indebted to Thomas Palberg and Hans Joachim Schöpe for carefully reading the manuscript, for their constructive criticism and many valuable suggestions to improve the manuscript. It is a pleasure to thank J Horbach and N Lorenz for stimulating discussions, H Reiber for particle synthesis, and the BW4-Team (A Timmann and S V Roth) at HASYLAB Hamburg for experimental support. Financial support of the Deutsche Forschungsgemeinschaft (He1601/17, 23, 24) is gratefully acknowledged.

References

- [1] Herlach D M, Galenko P and Holland-Moritz D 2007 *Metastable Solids from Undercooled Melts (Pergamon Materials Series)* ed R Cahn (Oxford: Pergamon)
- [2] Kelton K F and Greer A L 2009 *Nucleation (Pergamon Materials Series)* (Oxford: Pergamon)
- [3] Sood A 1995 *Solid State Phys.* **45** 1
- [4] Stöber W, Fink A and Bohn E 1968 *J. Colloid Interface Sci.* **26** 62
- [5] Yamanaka J, Yoshida H, Koga T, Ise N and Hashimoto T 1998 *Phys. Rev. Lett.* **80** 5806
- [6] Yamanaka J, Hayashi Y, Ise N and Yamaguchi T 1997 *Phys. Rev. E* **55** 3028
- [7] Wette P 2006 *PhD Thesis* Johannes Gutenberg-University Mainz
- [8] Schöpe H J and Palberg T 2001 *J. Colloid Interface Sci.* **234** 149
- [9] Wette P, Engelbrecht A, Sahl R, Klassen I, Menke D, Herlach D M, Roth S V and Schöpe H J 2009 *J. Phys.: Condens. Matter* **21** 464115
- [10] Klassen I 2009 *PhD Thesis* Ruhr-University Bochum
- [11] Roth S V *et al* 2006 *Rev. Sci. Instrum.* **77** 085106
- [12] Palberg T 1999 *J. Phys.: Condens. Matter* **11** 323
- [13] Lorenz N, Schöpe H J, Reiber H, Palberg T, Wette P, Klassen I, Herlach D M and Okubo T 2009 *J. Phys.: Condens. Matter* **21** 464116
- [14] Würth M, Schwarz J, Culis F, Leiderer P and Paberg T 1995 *Phys. Rev. E* **52** 6415
- [15] Monovoukas Y and Gast A P 1991 *Langmuir* **7** 460
- [16] Pan G, Sood A K and Asher A S 1998 *J. Appl. Phys.* **84** 83
- [17] Wette P, Schöpe H J and Palberg T 2005 *J. Chem. Phys.* **123** 174902
- [18] Aastuen D J W, Clark N A, Cottes L K and Ackerson B J 1986 *Phys. Rev. Lett.* **57** 2772
- [19] Palberg T 1999 *J. Phys.: Condens. Matter* **11** 323
- [20] Stipp A 2005 *PhD Thesis* Johannes Gutenberg University Mainz
- [21] Broughton J Q, Gilmer G H and Jackson A K 1982 *Phys. Rev. Lett.* **49** 1496
- [22] Willnecker R, Herlach D M and Feuerbacher B 1989 *Phys. Rev. Lett.* **62** 2707
- [23] Li D and Herlach D M 1996 *Phys. Rev. Lett.* **77** 1801
- [24] Wette P, Schöpe H J and Palberg T 2002 *J. Chem. Phys.* **116** 10981
- [25] Sirota E B, Ou Yang H D, Sinha S K, Chaikin P M, Axe J D and Fujii Y 1989 *Phys. Rev. Lett.* **62** 533
- [26] Cao C D, Letzig T, Görlner G P and Herlach D M 2001 *J. Alloys Compounds* **325** 113
- [27] Simonet V 1998 *PhD Thesis* Université de Paris-Sud UFR Scientifique d'Orsay, France
- [28] Simonet V, Hippert F, Klein H, Audier M, Bellissent R, Fisher H, Murani A P and Boursier D 1998 *Phys. Rev. B* **58** 6273
- [29] Simonet V, Hippert F, Audier M and Bellissent R 2001 *Phys. Rev. B* **65** 024203
- [30] Schenk T, Holland-Moritz D, Simonet V, Bellissent R and Herlach D M 2002 *Phys. Rev. Lett.* **89** 075507
- [31] Kelton K F, Lee G W, Gangopadhyay A K, Hyers R W, Rathz T, Rogers J, Robinson M B and Robinson D 2003 *Phys. Rev. Lett.* **90** 195504
- [32] Gasser U, Schofield A and Weitz D A 2003 *J. Phys.: Condens. Matter* **15** 375
- [33] Frank F C 1952 *Proc. R. Soc.* **215** 43
- [34] Turnbull D 1950 *J. Appl. Phys.* **21** 1022
- [35] Nelson D R and Spaepen F 1989 *Solid State Phys.* **42** 1
- [36] Klassen I, Wette P, Holland-Moritz D, Palberg T and Herlach D M 2010 at press
- [37] Holland-Moritz D, Schenk T, Bellissent R, Simonet V, Funakoshi K, Merino J M, Buslaps T and Reutzel S 2002 *J. Non-Cryst. Solids* **312–314** 47
- [38] Lee G W, Gangopadhyay A K, Kelton K F, Hyers R W, Rathz T J, Rogers J R and Robinson D S 2004 *Phys. Rev. Lett.* **93** 037802
- [39] Holland-Moritz D, Schenk T, Simonet V, Bellissent R, Couvert P and Hansen T 2002 *J. Alloys Compounds* **342** 77
- [40] Jonsson H and Andersen H C 1988 *Phys. Rev. Lett.* **60** 2295
- [41] Weeks J D, Chandler D and Andersen H C 2003 *J. Chem. Phys.* **54** 5237
- [42] Gasser U, Weeks E R, Schofield A, Pusey P N and Weitz D A 2001 *Science* **292** 8
- [43] Schall P, Cohen I, Weitz D A and Spaepen F 2006 *Nature* **440** 319
- [44] Harland J L and van Megen W 1997 *Phys. Rev. E* **55** 3054
- [45] Dobrich K M, Rau C and Krill C E 2004 *Metallurg. Mater. Trans. A* **35** 1953
- [46] Köster U and Schünemann U 1993 *Rapidly Solidified Alloys* ed H H Liebermann (New York: Dekker) p 303
- [47] Kelton K F 1991 *Solid State Phys.* **45** 75
- [48] Christian J W 1975 *The Theory of Transformations in Metals and Alloys* (Oxford: Pergamon) chapter 10
- [49] Turnbull D and Fisher J C 1949 *J. Chem. Phys.* **17** 71
- [50] Wette P and Schöpe H J 2007 *Phys. Rev. E* **75** 051405
- [51] Anderson V J and Lekkerkerker H N W 2002 *Nature* **416** 811
- [52] van Megen W 1995 *Transp. Theory Stat. Phys.* **24** 1017
- [53] Gillessen F, Herlach D M and Feuerbacher B 1987 *Z. Phys. Chem.* **156** 129
- [54] Marr D W and Gast A P 1993 *J. Chem. Phys.* **99** 2024
- [55] Wette P, Schöpe H-J, Liu H-J and Palberg T 2003 *Europhys. Lett.* **64** 124
- [56] Coriell S R and Turnbull D 1982 *Acta Metall.* **30** 2135
- [57] Barth M, Wei B and Herlach D M 1995 *Phys. Rev. B* **51** 3422
- [58] Köster U and Schünemann U 1993 *Rapidly Solidified Alloys* ed H H Liebermann (New York: Dekker) p 303
- [59] Kashchiev D 1969 *Surf. Sci.* **14** 209
- [60] Nash G and Glicksman M 1971 *Phil. Mag.* **24** 577
- [61] Nash G and Glicksman M 1969 *Acta Metall.* **17** 1
- [62] Turnbull D 1952 *J. Chem. Phys.* **20** 411
- [63] Turnbull D and Cech R E 1950 *J. Appl. Phys.* **21** 804
- [64] Klein S, Holland-Moritz D and Herlach D M 2009 *Phys. Rev. B* **80** 212202
- [65] Spaepen F 1975 *Acta Metall.* **23** 729
- [66] Spaepen F and Meyer R B 1976 *Scr. Metall.* **10** 257
- [67] Thompson C V 1979 *PhD Thesis* Harvard University
- [68] Holland-Moritz D 1998 *Int. J. Non-Equilib. Process.* **11** 169
- [69] Mermin N D 1965 *Phys. Rev. A* **127** 1509
- [70] Curtin W A 1989 *Phys. Rev. B* **39** 6775
- [71] Percus J K and Yevick G J 1958 *Phys. Rev.* **110** 1
- [72] Broughton J Q and Gilmer G H 1986 *J. Phys. Chem.* **84** 5749
- [73] Broughton J Q and Gilmer G H 1986 *J. Phys. Chem.* **84** 5759
- [74] Davidchack R L and Laird B B 2000 *Phys. Rev. Lett.* **85** 4751
- [75] Hoyt J J, Asta M and Karma A 2001 *Phys. Rev. Lett.* **86** 5530
- [76] Hoyt J J, Asta M, Haxhimali T, Karma A, Napolitano R E, Trivedi R, Laird B B and Morris J R 2004 *MRS Bull.* **29** 935

- [76] Schöpe H J, Bryant G and van Meegen W 2006 *Phys. Rev. Lett.* **96** 175701
- [77] Cacciuto A, Auer S and Frenkel D 2003 *J. Chem. Phys.* **119** 7467
- [78] Granasy L, Börzsönyi T and Pusztai T 2002 *Phys. Rev. Lett.* **88** 206105
- [79] Willnecker R, Herlach D M and Feuerbacher B 1988 *Mater. Sci. Eng. A* **98** 85
- [80] Mullis A M, Dragnevski K I and Cochrane R F 2004 *Mater. Sci. Eng. A* **375–377** 157
- [81] Herlach D M, Holland-Moritz D, Schenk T, Schneider K, Wilde G, Fransaer J and Spaepen F 1999 *J. Non-Cryst. Solids* **250–252** 271
- [82] McMullen W E and Oxtoby D W 1988 *J. Chem. Phys.* **88** 1967
- [83] Broughton J Q and Gilmer G H 1989 *J. Chem. Phys.* **84** 5749
- [84] Curtin W A 1989 *Phys. Rev. B* **39** 6775
- [85] Marr D W and Gast A P 1993 *J. Chem. Phys.* **99** 2024
- [86] Ohnesorge R, Loewen H and Wagner H 1994 *Phys. Rev. E* **50** 4801
- [87] Sun D Y, Asta M and Hoyt J J 2004 *Phys. Rev. B* **69** 174103